NF1 loss of function as an alternative initiating event in pancreatic ductal adenocarcinoma

Gopalakrishnan Ramakrishnan, Parash Parajuli, Pura Singh, Creighton Friend, Eric Hurwitz, Céline Prunier, Mohammed Razzaque, Keli Xu, Azeddine Atfi

Cell Reports

Article

NF1 loss of function as an alternative initiating event in pancreatic ductal adenocarcinoma

Graphical abstract

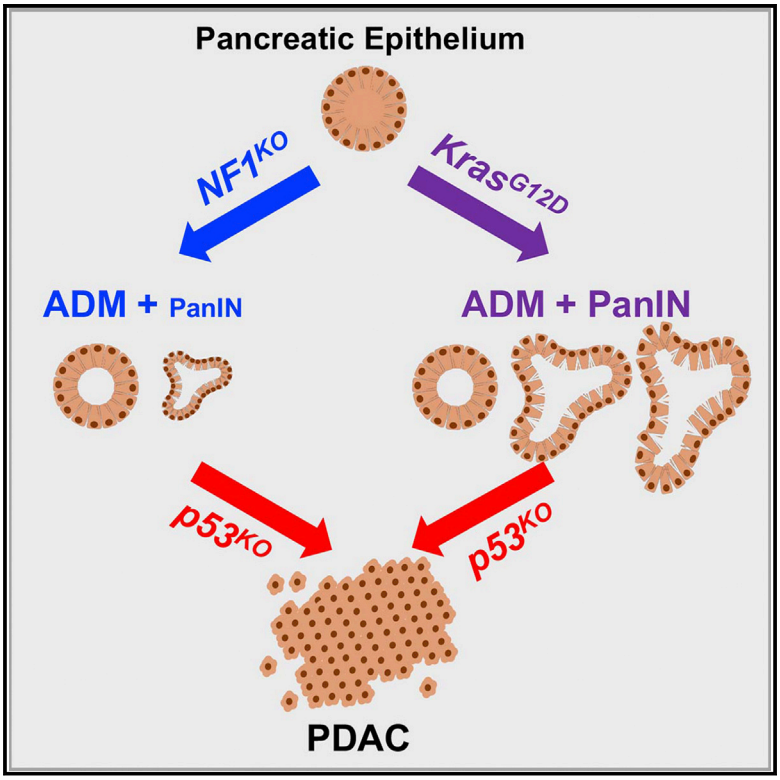

Authors

Gopalakrishnan Ramakrishnan, Parash Parajuli, Pura Singh, ..., Mohammed S. Razzaque, Keli Xu, Azeddine Atfi

Correspondence

azeddine.atfi@vcuhealth.org

In brief

Ramakrishnan et al. show that genetic inactivation of *NF1* can substitute for oncogenic *Kras* in driving PDAC pathogenesis and progression. As such, this finding unveils a long-sought-after mechanism leading to fatal PDAC in the substantial fraction of patients with normal *KRAS*.

Highlights

- NF1 expression is regulated by genetic mechanisms in PDAC
- *NF1* haploinsufficiency bolsters $Kras^{G12D}$-mediated PDAC initiation and progression
- The tumor suppressors p53 and PML regulate NF1 expression during PDAC progression
- Simultaneous inactivation of *NF1* and *p53* is sufficient to drive PDAC pathogenesis

Ramakrishnan et al., 2022, Cell Reports *41*, 111623
November 8, 2022
https://doi.org/10.1016/j.celrep.2022.111623

CellPress

Cell Reports

CellPress
OPEN ACCESS

Article

NF1 loss of function as an alternative initiating event in pancreatic ductal adenocarcinoma

Gopalakrishnan Ramakrishnan,[1,5] Parash Parajuli,[1,2] Pura Singh,[1] Creighton Friend,[2] Eric Hurwitz,[2] Celine Prunier,[3] Mohammed S. Razzaque,[4] Keli Xu,[1] and Azeddine Atfi[1,2,3,6,*]

[1]Cancer Institute, University of Mississippi Medical Center, Jackson, MS 39216, USA
[2]Department of Biochemistry & Molecular Biology and Massey Cancer Center, Virginia Commonwealth University, Richmond, VA 23298, USA
[3]Sorbonne Université, INSERM, CRSA, 75012 Paris, France
[4]Department of Pathology, Lake Erie College of Osteopathic Medicine, Erie, PA 16509, USA
[5]Present address: Department of Biochemistry & Molecular Biology, University of Illinois, Chicago, IL 60607, USA
[6]Lead contact
*Correspondence: azeddine.atfi@vcuhealth.org
https://doi.org/10.1016/j.celrep.2022.111623

SUMMARY

A long-standing question in the pancreatic ductal adenocarcinoma (PDAC) field has been whether alternative genetic alterations could substitute for oncogenic *KRAS* mutations in initiating malignancy. Here, we report that *Neurofibromin1* (*NF1*) inactivation can bypass the requirement of mutant *KRAS* for PDAC pathogenesis. An in-depth analysis of PDAC databases reveals various genetic alterations in the *NF1* locus, including nonsense mutations, which occur predominantly in tumors with wild-type *KRAS*. Genetic experiments demonstrate that *NF1* ablation culminates in acinar-to-ductal metaplasia, an early step in PDAC. Furthermore, *NF1* haploinsufficiency results in a dramatic acceleration of $Kras^{G12D}$-driven PDAC. Finally, we show an association between NF1 and p53 that is orchestrated by PML, and mosaic analysis with double markers demonstrates that concomitant inactivation of *NF1* and *Trp53* is sufficient to trigger full-blown PDAC. Together, these findings open up an exploratory framework for apprehending the mechanistic paradigms of PDAC with normal *KRAS*, for which no effective therapy is available.

INTRODUCTION

Pancreatic ductal adenocarcinoma (PDAC) is the fourth-leading cause of cancer-related deaths worldwide and one of the most aggressive malignancies.[1,2] Most PDAC patients present with inoperable disease and rapidly succumb to a devastating illness characterized by severe cachexia and general organ dysfunction.[2,3] The dismal hope of a cure comes from surgical resection in ~20% of patients who qualify, yet few survive beyond 5 years. Resistant to all current forms of therapies, advanced PDAC has a dismal 5-year survival rate of less than 7%.[1,2]

PDAC proceeds through a morphological spectrum of non-invasive lesions, known as acinar-to-ductal metaplasia (ADM) and pancreatic intraepithelial neoplasia (PanIN), accompanied by a recurrent pattern of genetic lesions, the earliest and most prevalent of which are activating mutations in the *KRAS* proto-oncogene, occurring in up to 90% of patients.[4,5] Given its high incidence at very early stages of the disease, mutational activation of *KRAS* has been postulated as the key genetic determinant for PDAC initiation. Other subsequent inactivating mutations in the tumor-suppressor genes *p16INK4A*, *SMAD4*, and *TP53* (referred to hereafter as *p53*) are deemed essential for PDAC to progress and metastasize.[5–7] In line with the human genetic alterations, pancreas-specific expression of $Kras^{G12D}$ in mice is sufficient to initiate ADM and attendant PanINs, which occasionally progress into invasive PDAC following a long latency period.[8,9] Importantly, combining $Kras^{G12D}$ with inactivation of *p16Ink4a*, *Smad4*, or *Trp53* (referred to hereafter as *p53*) has been shown to accelerate the development of PDAC tumors with clinical and physiopathological features that closely recapitulate the human disease.[10–13]

Kras belongs to the Ras superfamily of small GTPases, which serve as molecular switches to mediate a variety of signal cues key to cell growth and function.[14] Ras proteins cycle between an active guanosine 5′-triphosphate (GTP)-bound state and an inactive guanosine 5′-diphosphate (GDP)-bound state. This is mediated by nucleotide-exchange factors, which catalyze the exchange of GDP for GTP, and GTPase-activating proteins (GAPs), which potentiate the weak Ras intrinsic GTPase activity.[15,16] *RAS* family members are the most frequently mutated oncogenes in human cancer. Mutations in *KRAS* are more prevalent than those in *NRAS* or *HRAS*, and occur predominantly in the adenocarcinomas of pancreas, colon, and lung.[17] Single-base substitutions in *RAS* genes often occur in codon 12 and much less frequently in

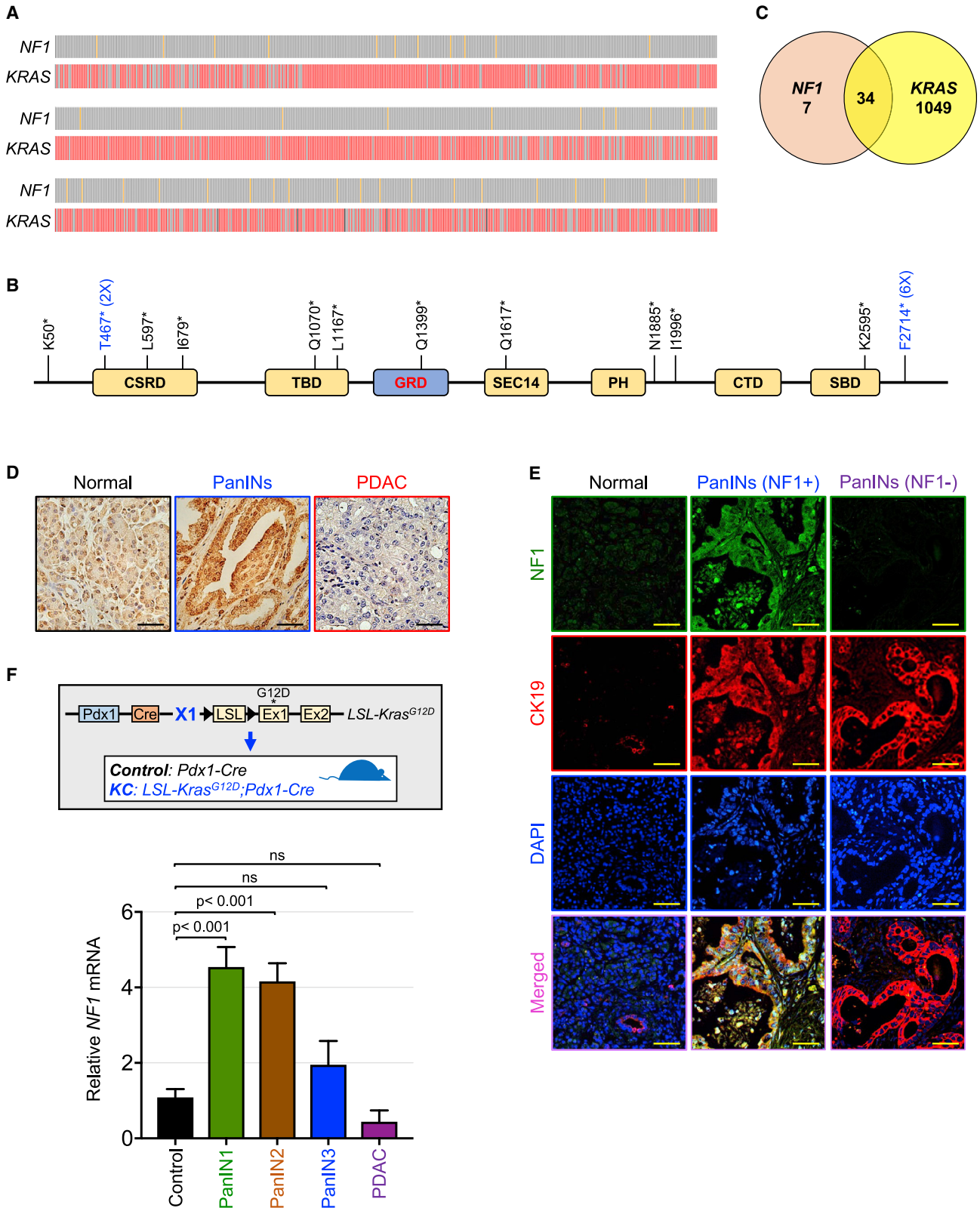

(legend on next page)

codons 13 and 61.[18] Codon 12 mutations have been postulated for decades to render Ras proteins insensitive to the hydrolyzing activity of GAPs, thus causing them to remain chronically active.[19] However, such view was recently challenged by new pharmacological studies revealing that the $Kras^{G12C}$ mutant retains hydrolytic activity and continues to cycle between its active and inactive states.[20] Despite adding extra complexity to the intricate model of Ras regulation, this recent progress offers a unique opportunity for exploring new approaches to counter mutant Kras, which has so far proven to be intractable.[21]

The *NF1* tumor-suppressor gene encodes Neurofibromin-1, a GAP protein that specifically promotes the conversion of the active Ras-GTP bound form to its inactive Ras-GDP bound form, therefore functioning as a general negative regulator of Ras oncoproteins.[22,23] Germline mutations or microdeletions in *NF1* are responsible for neurofibromatosis type 1, also known as von Recklinghausen disease, a dominant inherited genetic disease that predisposes patients to a variety of cancers, including neurofibromas, glioblastomas, and pheochromocytomas.[24] In the vast majority of NF1-deficient tumors, constitutive activation of Ras signaling has been noted, supporting the general notion that NF1 might fulfill its tumor-suppressive function in part by inactivating Ras signaling.[24] Notwithstanding this progress in understanding NF1 biology, it remains unclear whether *NF1* inactivation operates independently or simultaneously with oncogenic Ras signaling to promote cancer pathogenesis, progression, or both. In this study, we undertook a variety of orthogonal and genetic approaches to address this question, focusing on PDAC, where we identified frequent genetic alterations in *NF1*, occurring either separately or simultaneously with *KRAS* mutations. We found that ablating *NF1* resulted in a dramatic acceleration of $Kras^{G12D}$-driven PDAC, suggesting that NF1 might function to restrain the oncogenic capabilities of mutant *Kras*. Interestingly, ablating *NF1* along with *p53* in a wild-type *Kras* background was sufficient to drive the formation of invasive PDAC, suggesting that *NF1* loss of function might bypass the requirement for oncogenic *Kras*. Thus, by demonstrating that concomitant inactivation of *NF1* and *p53* can substitute for oncogenic *Kras* in PDAC, our findings shed light on a previously unrecognized mechanism leading to PDAC pathogenesis and progression in the substantial fraction of PDAC patients with normal *KRAS*.

RESULTS

NF1 genetic alterations in human PDAC

Interrogation of several public databases (see STAR Methods) revealed the presence of various alterations in the *NF1* gene in a significant proportion of human PDAC tumors, ranging from 3.4% to 24.6% (all alterations), depending on the dataset scrutinized (Figures S1A and S1B and Table S1). Among the 1,471 samples analyzed, 41 (2.40%) harbored either nonsense or missense mutations (Figure 1A and Table S1). Copy number variations (CNVs) do not seem to account significantly for *NF1* alterations, as only one tumor harbors a deletion in the *NF1* locus. Of critical importance, the majority of missense mutations are predicted to have strong damaging effects on NF1 activity (Table S1). Furthermore, among the 18 nonsense mutations found in *NF1*, 8 (44.44%) are likely to culminate in truncated proteins lacking the catalytic Ras GTPase-activating domain (Figure 1B). Finally, 7 of these 8 tumors with *NF1* nonsense mutations harbor wild-type *KRAS* (Figure 1C and Table S1), hinting at the possibility that *NF1* genetic inactivation might represent an alternative driver event in PDAC.

To explore whether there are any additional mechanisms affecting NF1 function in PDAC, we performed immunohistochemistry (IHC) experiments using a highly specific anti-NF1 antibody (see Figure 2B) to probe for NF1 protein expression in three different tissue microarrays (TMAs) comprising 179 samples confirmed as either normal (65) or PDAC (114) with PanINs and full PDAC lesions. As shown in Figure 1D, NF1 expression initially increased in PanIN lesions, but subsequently dropped to background levels in PDAC lesions, suggesting that NF1 might be transiently expressed during PDAC progression. A double-blinded quantification of staining intensity showed that about 64% of PanINs displayed the highest levels of NF1 expression, whereas less than 5% of PDAC lesions reached the same degree of NF1 expression as in PanINs (Figure S1C). Nonetheless, it should also be noted that about 18% of PanINs were almost completely devoid of any NF1 expression, an observation that we subsequently validated through co-immunofluorescence (co-IF) using antibodies to the ductal marker cytokeratin-19 (CK19) and NF1 (Figures 1E and S1C). Although the presence of mutations in *NF1* could by itself explain the lack of NF1 expression in those PanINs, we did not rule out the involvement of additional mechanisms, such as inactivation of *p53*, *p16INK4A*, and *SMAD4* (Table S1).

To further understand the mechanisms influencing NF1 expression during PDAC progression, we sought to utilize genetically engineered mouse models (GEMMs) that recapitulate various aspects of the human PDAC disease in a uniform genetic background.[8,9,13,25] We generated mice with pancreas-specific expression of $Kras^{G12D}$ alone (*KC*) or together with homozygous deletion of *p53* (*KPC*), *p16Ink4a* (*KIC*), or *Smad4* (*KSC*). Except for *KPC* mice, we detected transient expression of NF1 in pancreatic sections from all other genotypes analyzed (Figure S1D), similar to what was observed in human PDAC. We also extended our approaches to analyze *NF1* mRNA expression in cohorts of increasingly aged *KC*

Figure 1. NF1 genetic alterations in PDAC

(A) Oncoplot showing genetic coding alterations in *NF1* and *KRAS* in human PDAC samples found in several public datasets, as described in STAR Methods.

(B) Distribution of PDAC nonsense mutations identified in *NF1*. The recurrent mutations are highlighted in blue.

(C) Numbers of overlapping and independent PDAC mutations in *NF1* and *KRAS* of samples shown in (A).

(D and E) NF1 and/or cytokeratin-19 (CK19) expression was analyzed by immunohistochemistry or co-immunofluorescence using three different human TMAs. Representative pictures are shown. Scale bars: (D) 25 and (E) 50 μm.

(F) NF1 expression was analyzed by qRT-PCR using pancreatic tissues from control (2 months) and *KC* mice with progressive PanIN (2 months for PanIN1, 4 months for PanIN2, 6 months for PanIN3) and PDAC (12 months) lesions (n = 6; 3 females and 3 males). Data are expressed as the mean ± SEM.

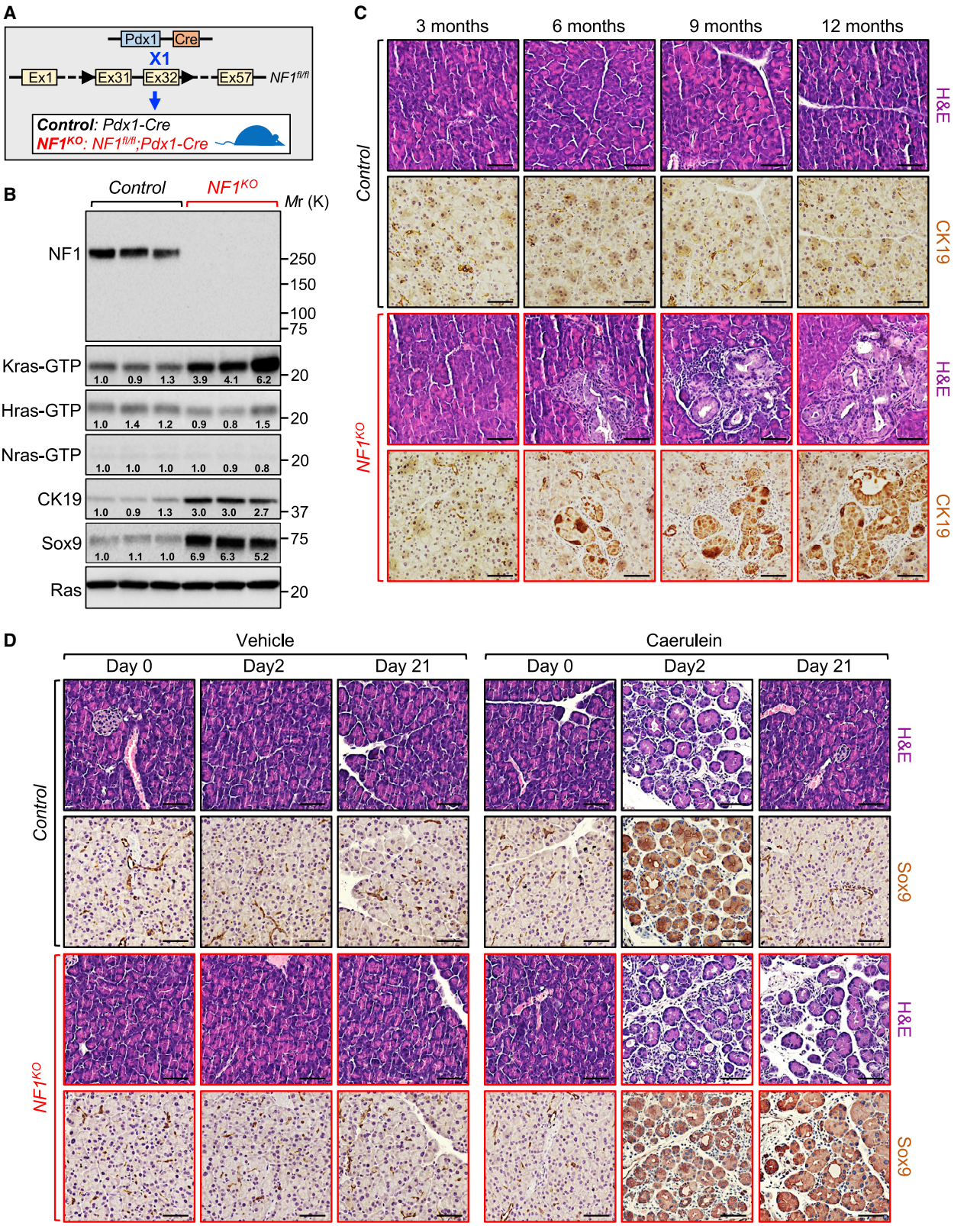

(legend on next page)

mice, which we have previously characterized in terms of the relative abundance of PanIN or PDAC lesions.[26,27] The result showed that *NF1* expression was markedly upregulated in *KC* mice with PanIN1 and PanIN2 but that that increase had commenced to level off in mice with PanIN3 and reached less than 30% of the normal level in mice with PDAC lesions (Figure 1F). When taken together with the clinical data, these findings suggest the existence of genetic and epigenetic events that influence the expression of the tumor suppressor NF1 in PDAC. In addition, given the transient expression of NF1 during PDAC progression, it is conceivable that NF1 might orchestrate a tumor-suppressive barrier to restrict the progression to PDAC; we will return to this notion later. We will also return to provide an explanation as to why *KPC* mice lack the typical transient expression of NF1 observed during PDAC progression.

NF1 deficiency triggers ADM

To delineate a possible role of NF1 in PDAC, we generated mice with pancreas-specific deletion of *NF1* (referred to hereafter as $NF1^{KO}$) by crossing mice bearing a floxed allele of *NF1* with *Pdx1-Cre* mice (Figure 2A), which express Cre recombinase in all pancreatic progenitor cells, including islet, ductal, and acinar cells.[28] $NF1^{KO}$ mice were born at the expected Mendelian ratio, showed no evidence of any gross anatomic abnormalities, and had normal body weight and life expectancy (Figure S2B). Further analysis showed that *NF1* deletion had no apparent effects on islet integrity or function, as evidenced by the comparable immunostaining of insulin and glucagon as well as the normal blood glucose levels in $NF1^{KO}$ mice relative to their wild-type littermates (Figures S2C and S2D). Immunoblot analysis confirmed the loss of NF1 expression in $NF1^{KO}$ mice (Figure 2B). Moreover, *NF1* deletion led to a significant increase in Kras-GTP (Figure 2B), consistent with its well-established role as a suppressor of Ras signaling.[22,23] Of note, *NF1* deletion did not increase the levels of Hras-GTP or Nras-GTP (Figure 2B), suggesting that NF1 might specifically target Kras in the pancreatic epithelium.

Despite the apparently normal phenotype of $NF1^{KO}$ mice, we noticed that the acinar parenchyma of mice aged 6 months and older consistently displayed morphological changes reminiscent of ADM (Figure 2C), the earliest lesion found in human PDAC.[29] ADM is known to increase the propensity for neoplasia and is associated with oncogenic *KRAS* transformation as well as pancreatitis. During ADM, acinar cells lose their identity and undergo a process of transdifferentiation into the ductal lineage, accompanied by the de-repression of the ductal genes *CK19* and *Sox9*.[29,30] As gauged by immunoblotting, we observed a marked increase in the expression of CK19 and Sox9 upon *NF1* deletion (Figure 2B). We also conducted IHC experiments and detected lesions that exhibit high affinity to the anti-CK19 antibody (Figure 2C), providing further evidence that *NF1* inactivation can drive ADM formation, as does oncogenic $Kras^{G12D}$[31] (see also Figure S2E). It is noteworthy that we noticed that NF1 deficiency in aged mice occasionally resulted in the formation of structures resembling PanIN1 that stained positive for CK19 (Figure 2C), although those lesions have never progressed to fatal PDAC in more than 62 mice analyzed.

To investigate in more depth the physiopathological consequence of this phenotype, we focused our effort on pancreatitis, which is known to engender an inflammatory milieu that promotes the rapid progression from benign ADM/PanIN to invasive PDAC in the background of $Kras^{G12D}$.[31,32] As shown in Figure 2D, intraperitoneal administration of the pancreatitis-inducing agent caerulein[31,32] to 2-month-old mice drove similar damage in the acinar parenchyma of $NF1^{KO}$ mice and their wild-type littermates within 48 h (Figure 2D). Following a period of 3 weeks of healing, caerulein-treated control mice had remarkably repaired the induced damage with physiology akin to that of the vehicle, whereas caerulein-treated $NF1^{KO}$ mice displayed numerous ADM/PanIN lesions (Figure 2D). As with aged $NF1^{KO}$ mice (Figure 2C), the accelerated ADM/PanIN lesions failed to progress to lethal PDAC within an observation period exceeding 12 months (Figure S2F). As a specificity control, all caerulein-treated *KC* mice succumbed to invasive PDAC within 6 months following caerulein treatment (Figures S2F and S2G).

NF1 haploinsufficiency accelerates $Kras^{G12D}$-driven PDAC

The data obtained so far showed that inactivation of *NF1* in a *Kras* wild-type background was able to trigger ADM and, occasionally, early PanINs, yet these lesions do not progress to PDAC even in the context of pancreatitis, raising the question as to whether mutational inactivation of *NF1* would require additional genetic alterations to initiate and/or exacerbate PDAC. Since our earlier analysis revealed the co-occurrence of *NF1* and *KRAS* mutations in human PDAC tumors (Figure 1C), we sought to explore whether *NF1* inactivation could facilitate $Kras^{G12D}$-driven PDAC. To do so, we set out to generate mice with the combined expression of $Kras^{G12D}$ and homozygous deletion of *NF1* in the pancreatic epithelium. Despite several attempts using different breeding schemes, we were not able to obtain mice that survive beyond birth, indicative of the lethality of this genetic combination. To overcome this limitation, we examined mice with $Kras^{G12D}$ and heterozygous deletion of *NF1* (referred to hereafter as *KNC* mice). As shown in Figure 3A, deleting one copy of *NF1* (*NC* mice) did not have any visible effect on pancreas histology, indicating that *NF1* haploinsufficiency is not sufficient to drive ADM. Strikingly, however, deleting one copy of *NF1* completely transformed the indolent PanIN lesions seen with $Kras^{G12D}$ alone, forcing them to progress into

Figure 2. *NF1* ablation leads to ADM

(A) Schematic representation of genetically engineered mouse models (GEMMs) of PDAC used in the experiments.

(B) Immunoblot analysis of PDAC-relevant proteins in pancreatic extracts from $NF1^{KO}$ mice and their wild-type littermates (n = 3; 2 females and 1 male).

(C) Analysis of pancreatic tissues from control or $NF1^{KO}$ mice at different ages (3, 6, 9, or 12 months) by hematoxylin and eosin (H&E) or immunohistochemistry using anti-CK19 antibody. Representative pictures are shown (n = 6; 3 females and 3 males). Scale bars: 50 μm.

(D) Two-month-old control or $NF1^{KO}$ mice were treated with vehicle or caerulein, and pancreas histology was analyzed by H&E or immunohistochemistry using anti-Sox9 antibody. Representative pictures are shown (n = 6; 3 females and 3 males). Scale bars: 50 μm.

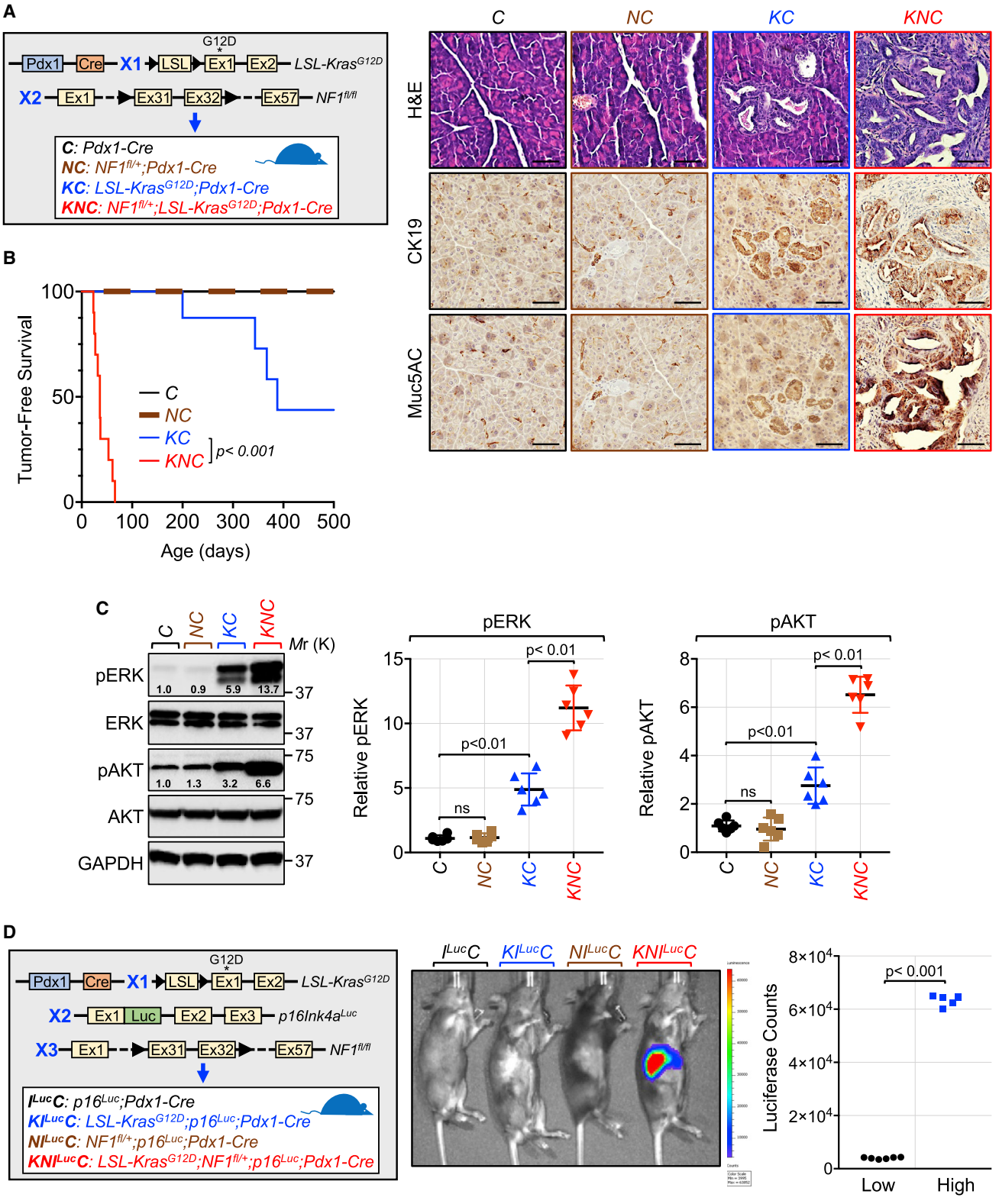

Figure 3. *NF1* haploinsufficiency accelerates Kras^{G12D}-driven PDAC

(A) Pancreatic tissues from 6-week-old mice highlighted in the schematic (left) were analyzed by H&E or immunohistochemistry using antibodies to CK19 and Muc5AC (right). Representative pictures are shown (n = 6; 3 females and 3 males). Scale bars: 50 μm.

(legend continued on next page)

full-blown PDAC with an accelerated course (Figures 3A and 3B), similar to what was observed in other studies with homozygous deletion of *p53* (*KPC*), *Smad4* (*KSC*), or *p16Ink4a* (*KIC*).[10–13] *KNC* mice were stunted and morbid in appearance, often succumbing to the disease within 4 weeks without any visible signs of metastasis, and none of them survived beyond 10 weeks (Figure 3B). Phenotypically, the tumors displayed the prominent hallmarks of PDAC, as assessed by immunostaining using antibodies to CK19 and Muc5AC (Figure 3A). In addition, the tumors showed uniformly poorly differentiated architectures, exhibiting high proliferative behavior as well as extensive epithelial-to-mesenchymal transdifferentiation (EMT) and angiogenesis (Figure S3A). At the same age, *KC* mice consistently showed the presence of PanIN lesions, exhibiting only sparse proliferation, and little to no sign of EMT and angiogenesis (Figures 3A and S3A). The aggressive nature of the PDAC tumors in *KNC* mice was also reflected in the synergistic effects on Kras-GTP as well as the downstream ERK and AKT pathways (Figures 3C, S3A, and S3B). Interestingly, these phenotypes appeared to occur without loss of heterozygosity at the *NF1* gene (Figures S3C and S3D), indicating that the *NF1* gene dosage is sufficient to accelerate PDAC.

To corroborate this finding, we performed genetic experiments using the *p16Ink4a-Luciferase* ($p16^{Luc}$) mouse model, which puts luciferase under the control of the endogenous *p16Ink4a* promoter and in a manner to disrupt *p16Ink4a* but to leave *p19Arf* intact.[33] When combined with oncogene activation or tumor-suppressor gene inactivation, the $p16^{Luc}$ allele allows for simple, serial, and noninvasive evaluation of p16 expression, which represents an unbiased assessment of tumor emergence, as $p16^{Luc}$ is expressed exclusively during malignant transformation and aging.[33] We generated four cohorts of mice harboring one copy of the $p16^{Luc}$ allele and monitored luciferase expression in live animals by IVIS imaging (Figure 3D). We detected bioluminescence in $KNI^{Luc}C$ mice as early as 4 weeks after birth, an age at which $I^{Luc}C$, $KI^{Luc}C$, or $NI^{Luc}C$ mice have never showed any luciferase expression. Collectively, these data provide strong evidence that *NF1* haploinsufficiency accelerates $Kras^{G12D}$-driven PDAC.

Next, we wondered whether NF1 could exert its tumor-suppressive function in a cell-autonomous manner. To probe this possibility, we initially employed the human PDAC cell line MIA PaCa-2, which has been shown to retain addiction to endogenous $Kras^{G12C}$ expressed from both *KRAS* alleles.[34] Using two different gRNAs targeting $KRAS^{G12C}$, we independently confirmed that these cells are addicted to the $Kras^{G12C}$ oncoprotein (Figures S4A–S4C). Interestingly, inducing NF1 expression in MIA PaCa-2 cells expressing a doxycycline-inducible NF1 cDNA was able to inhibit cell proliferation to an extent approaching that elicited by $KRAS^{G12C}$ ablation (Figures S4D and S4E). This effect is likely to be mediated via suppression of Ras signaling, as transducing cells with a retrovirus encoding $Kras^{G12C}$ was able to rescue proliferation in cells overexpressing NF1 (Figures S4D and S4E). In an alternative approach, we performed cell transformation experiments using the human immortalized pancreatic epithelial cell line (HPDE), which has been shown to retain a normal phenotype following $Kras^{G12D}$ expression.[35] We generated isogenic HPDE cell lines with either expression of $Kras^{G12D}$ alone (*K*) or deletion of *NF1* alone ($NF1^{KO}$) or both ($KNF1^{KO}$) (Figure 4A). We did not observe any change in cell morphology when $Kras^{G12D}$ expression and *NF1* deletion were conducted separately (Figure 4B). However, combining $Kras^{G12D}$ expression with *NF1* deletion led to a dramatic change in cell morphology reminiscent of malignant transformation. In fact, $KNF1^{KO}$ cells began to form floating colonies that continued to grow without attaching to the matrix and could be passaged indefinitely while retaining almost 100% viability (Figures 4B and S4F), indicative of the acquisition of a malignant and invasive phenotype. The ability of $KNF1^{KO}$ cells to form floating colonies was almost completely canceled by adding back NF1 (Figure S4H). We also observed increased cell proliferation and EMT as well as upregulation of Kras-GTP and ERK/AKT activities in $KNF1^{KO}$ cells compared with *K* or $NF1^{KO}$ cells (Figures 4A, 4C, and S6G). When taken together with our *in vivo* genetic experiments, these findings suggest that *NF1* inactivation might contribute to PDAC development and progression via a cell-autonomous mechanism.

Association between NF1 and p53 in PDAC

Inactivating mutations in the *p53* tumor locus are among the well-known acquired secondary mutations that confer an invasive phenotype to PDAC.[7,36] Since our earlier findings have revealed that *NF1* was also significantly mutated in human PDAC, we sought to extend our analyses to investigate whether there is any association between *NF1* and *p53*, and if so, whether this has any significance for PDAC pathogenesis and progression. Analysis of human datasets showed that a small fraction (1.7%) of the tumors with *p53* mutations harbor mutations in *NF1* (Figures 5A, 5B, and S5A). In marked contrast, a significant proportion (62.3%) of the tumors with *NF1* mutations harbor mutations in *p53*, raising the possibility that NF1 might function as a tumor suppressor in PDAC through a mechanism necessitating the simultaneous inactivation of *p53*. To explore further a possible association between NF1 and p53, we analyzed p53 and NF1 protein expression by IHC and co-IF, employing the three human PDAC TMAs described earlier. We found that expression of p53 exhibited a trend akin to that of NF1 in 72% of samples, commencing with low levels in normal pancreas, then rising in PanINs, and finally declining to the background level in PDAC (Figures 5C–5E and S5B). The remaining 28% of samples showed very high expression of p53, although the underlying mechanism is unclear, as the TMAs do not show any information about *p53* mutational status. Nevertheless, it is

(B) Kaplan-Meier analysis of survival of mice with the indicated genotypes (n = 12–21; 7–10 females and 5–11 males).
(C) Pancreatic extracts from 6-week-old mice with the indicated genotypes were analyzed for pERK or pAKT. A representative immunoblot is shown on the left. Right: the graphs show the quantification of six samples from each genotype (n = 6; 3 females and 3 males).
(D) PDAC growth in 2-month-old mice (3 females and 3 males) with the indicated genotypes highlighted by the scheme (left) was analyzed by IVIS bioluminescence. Representative luciferase images are shown (middle). Right: the graph shows the minimum and maximum of luciferase counts recorded in six experiments.

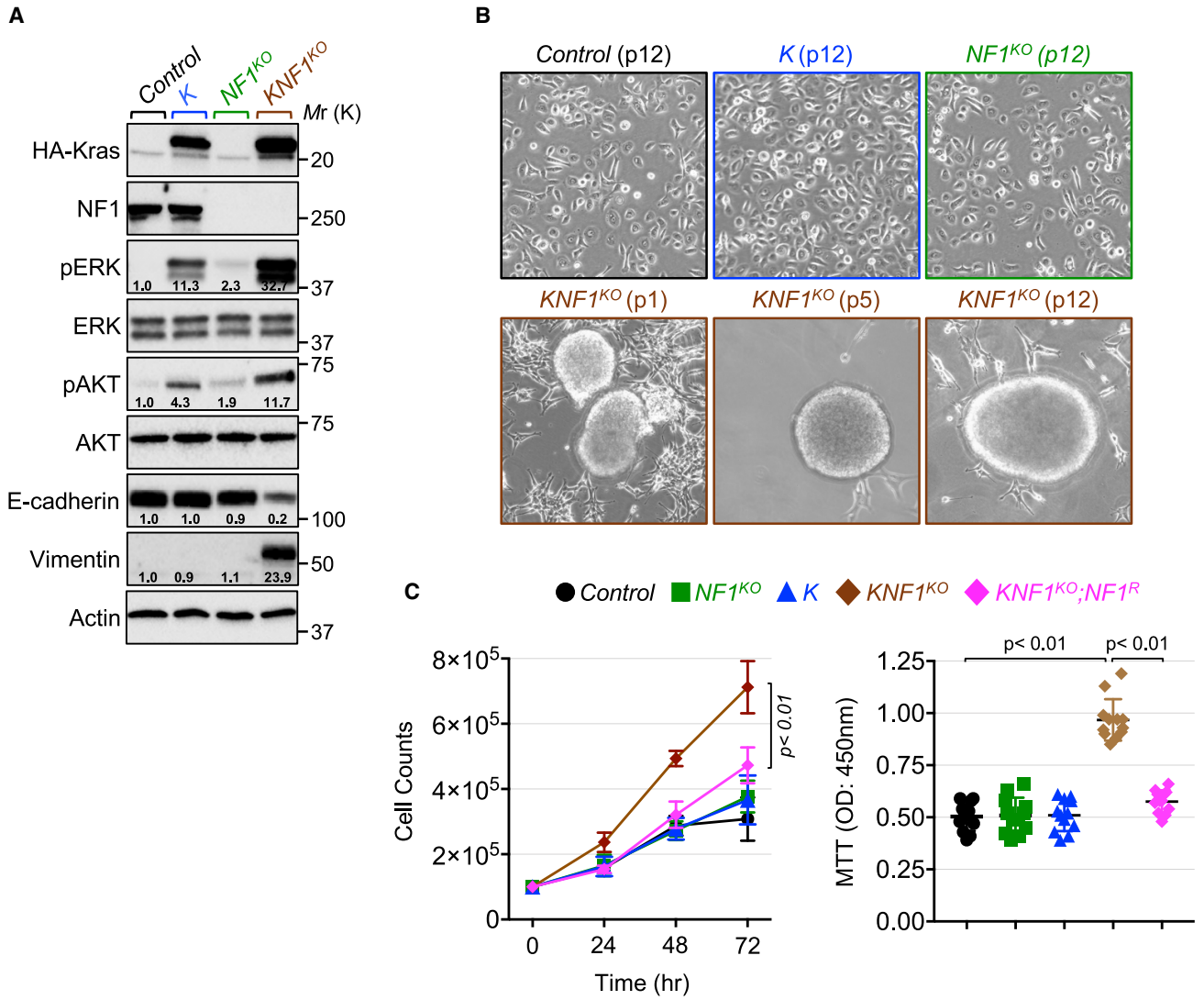

Figure 4. NF1 restricts PDAC growth via a cell-autonomous mechanism

(A–C) Isogenic HPDE cell lines stably expressing various combinations of HA-Kras^{G12D} and gRNA targeting *NF1* were analyzed for HA-Kras^{G12D}, NF1, pERK, ERK, pAKT, AKT, and β-actin expression by immunoblotting (A). Cells were passaged 12 times, and representative pictures of cells or spheres at different passages are shown (B). Cell proliferation was assessed either by cell counting at different time periods or by MTT after 96 h in culture (C). Data in (C) are expressed as the mean ± SEM.

conceivable that this effect might be due to the presence of mutations that are known to simultaneously inactivate and stabilize p53.[37,38] Regardless, the 28% of samples with high p53 expression express low levels of NF1, providing an initial indication that the association between p53 and NF1 during PDAC progression might depend on p53 transcriptional activity. To substantiate this hypothesis, we utilized our PDAC GEMMs (e.g., *KC*, *KIC*, *KSC*), which mimic the pathophysiological features of the human disease in a uniform genetic background. We found that p53 protein expression closely mirrored that of NF1 in both normal and cancerous areas in 100% of samples analyzed (Figure S5C). This conclusion also holds true when the expression of *p53* mRNA was analyzed in *KC* mice with the progressive abundance of PanIN and PDAC lesions (Figures 1F and S5D).

To confirm these findings, we conducted comparative qRT-PCR experiments to quantify *NF1* mRNA expression in *KPC* and *KC* mice described earlier. In line with the IHC data, *KPC* mice displayed a significant decrease (1.8-fold) in *NF1* expression compared with their wild-type littermates (Figure S5E). On the other hand, *KC* mice displayed a 3.8-fold increase in *NF1* expression relative to control animals, further supporting the ability of p53 to regulate NF1 expression during PDAC progression. We also generated *KC* mice in the background of mice with a reactivable allele of *p53* (*KrPC^{Tam}*) (Figure 5F), which contain a Loxp-Stop-Loxp cassette knocked into the endogenous *p53* allele and behave as a global knockout.[39] In these mice, expression of endogenous p53 is restored only in cells expressing Cre recombinase, thus eliminating any interference

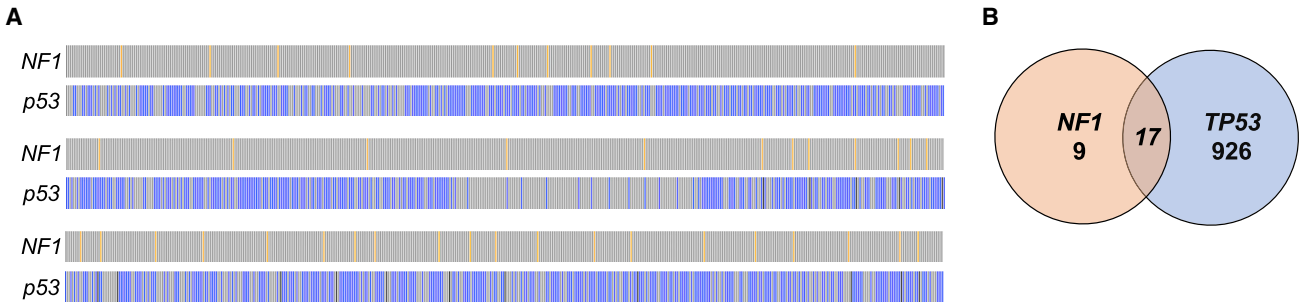

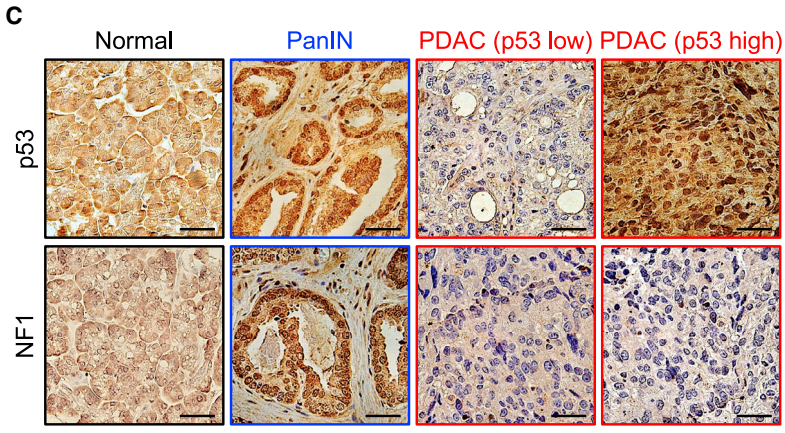

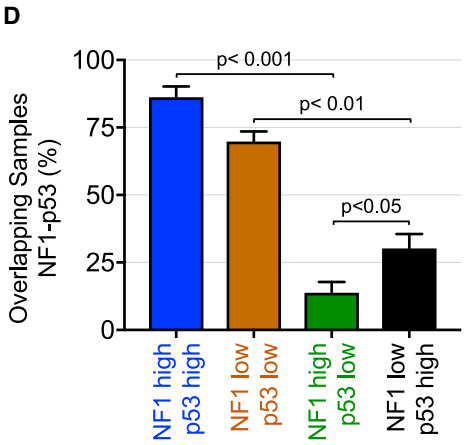

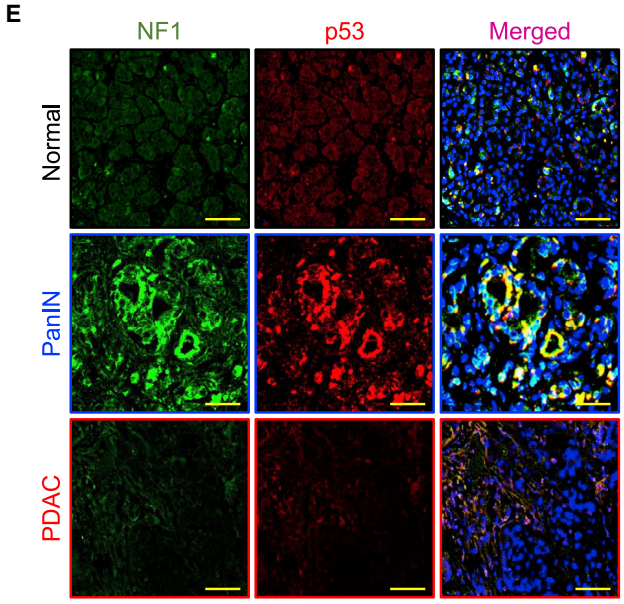

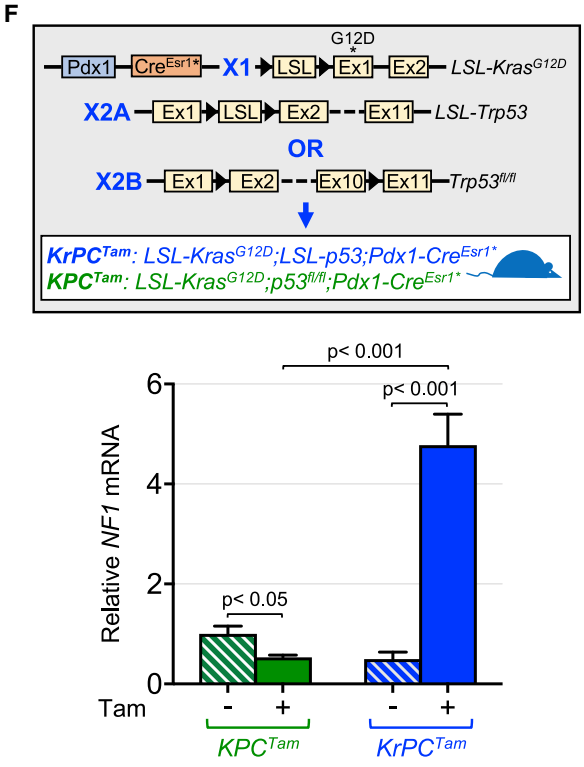

(legend on next page)

from the stroma or infiltrating immune cells, which in principle express p53 in the *KPC* background. To restore p53 expression, we used *Pdx1-Cre*^{ERT2} mice, in which Cre recombinase is activated by tamoxifen, thus enabling the controlled expression of p53 early during PDAC development. *KPC*^{Tam} mice were used as controls (Figure 5F). Upon tamoxifen (Tam) treatment, *KrPC*^{Tam} mice displayed a marked increase (4.5-fold) in *NF1* expression, whereas *KPC*^{Tam} displayed the opposite response (1.8-fold decrease) (Figure 5F). Finally, we assessed p53 expression in mice with pancreas-specific homozygous deletion of *p53* (*p53*^{KO}) to investigate whether p53 could regulate NF1 expression under normal conditions. Mice with conditional deletion of one (*NC*) or two (*NF1*^{KO}) alleles of *NF1* were used as reference controls (Figure S5F). We observed a 1.7-fold decrease in *NF1* expression in *p53*^{KO} mice compared with their wild-type littermates (Figure S5F). This decrease was slightly lower than the decrease (1.9-fold) observed in mice with one allele of *NF1* deleted, suggesting that additional mechanisms might regulate NF1 expression. As anticipated, *NF1* mRNA expression in mice with both *NF1* alleles deleted was below the detection threshold in the vast majority of mice analyzed (Figure S5F). In the course of this analysis, we also found that deleting *NF1* did not affect p53 expression even under PDAC conditions (Figures S3E and S5F), arguing again the possibility that NF1 might regulate p53 expression in a reciprocal manner. Collectively, these genetic approaches provide compelling evidence that p53 regulates NF1 expression under both normal and PDAC conditions.

NF1 as an indirect p53 target gene

The above-mentioned data prompted us to explore whether p53 could regulate NF1 expression. Accordingly, we generated MIA PaCa-2 cells stably expressing a doxycycline-inducible p53 cDNA and examined NF1 expression. We found that treating these cells with doxycycline (Dox) elicited a marked increase in both NF1 protein and mRNA expression (Figures 6A and S6A). A similar p53-mediated NF1 expression was also observed in the human PDAC cell line Panc-1 (Figure S6B). We also generated MIA PaCa-2 cell lines stably expressing Dox-inducible p53 with two "hotspot" mutations, R248Q and R273H, which are known to stabilize and disable normal p53 transcriptional activity.[37] Compared with wild-type p53, these mutants failed to induce NF1 expression despite being expressed at levels exceeding that of wild-type p53 (Figure S6C). This observation not only suggests that p53 transcriptional activity is required for the regulation of NF1 expression, but also explains why NF1 expression was barely detectable in a fraction (28%) of human PDAC samples displaying high levels of p53, perhaps due to the presence of inactivating/stabilizing mutations in p53.

To understand the mechanisms by which p53 regulates NF1 expression, we interrogated the Eukaryotic Promoter Database for the active promoter region in the *NF1* gene. However, we were not able to find any p53 binding sequence,[40] suggesting that p53 might regulate NF1 indirectly. To probe this possibility, we generated reporter constructs in which luciferase was under the control of 400-bp fragments that tiled across the entire *NF1* promoter (1,088 bp) with a 200-bp overlap and tested for their sensitivity to p53 using MIA PaCa-2 cells. Transfecting p53 drove luciferase expression exclusively from two reporters with overlapping fragments (Figure S6D), confirming the ability of p53 to regulate NF1 expression and further narrowing down the p53-responsive region to 200 bp. When this 200-bp fragment was further divided into two 100-bp fragments and examined for their sensitivity to p53, only two conserved binding sites for the transcription factors PML and TFAP2C were present in the fragment that responded to p53 (Figures S6E and S6F). In subsequent experiments, we obtained several lines of evidence that PML mediates p53-induced NF1 expression. First, chromatin immunoprecipitation (ChIP) assays showed that PML associated strongly with the *NF1* promoter in mouse embryonic fibroblasts (MEFs) from wild-type mice (*PML*$^{+/+}$), but not in MEFs from mice with PML deleted (*PML*$^{-/-}$) (Figure 6B). Second, expressing p53 in *PML*$^{-/-}$ MEFs failed to induce the *NF1* luciferase reporter, compared with *PML*$^{+/+}$ MEFs (Figure 6C). The effect of p53 in the presence of PML is specific, as expression of three p53 hotspot mutants, p53.R248Q, p53.R172H, and p53.R273H, had little or no effect on the NF1 reporter (Figure 6C). Third, mutating the binding site of PML, but not that of TFAP2C, completely blocked luciferase expression in response to p53 (Figure S6F). Fourth, inducing p53 expression had little or no effect on NF1 protein expression in MIA PaCa-2-Dox-HA-p53 cells with *PML* deleted by CRISPR-Cas9, compared with their PML-sufficient counterparts (Figure 6D). Reconstitution of these cells with a gRNA-resistant form of PML restored responsiveness to p53 (Figure 6D). Fifth, since PML has been shown to interact with and modulate p53 transcriptional activity as it relates to its tumor-suppressive functions,[41,42] we considered the possibility that PML might recruit p53 to the *NF1* promoter. Accordingly, we conducted ChIP experiments using MIA PaCa-2-Dox-HA-p53 cells and their isogenic variants with *PML* deleted. We found that PML strongly interacted with the *NF1* promoter irrespective of whether cells were cultured in the absence or presence of Dox (Figures 6E and 6F). In contrast, p53 interacted with the *NF1* promoter only in cells that had been exposed to Dox (Figures 6E and

Figure 5. Association between NF1 and p53 in PDAC

(A) Oncoplot showing coding genetic alterations in *NF1* and *p53* in human PDAC samples found in public datasets.

(B) Numbers of overlapping or independent PDAC mutations in *NF1* and *TP53* in samples shown in (A). *TP53* mutational status is not known in the 14 samples with *NF1* mutations.

(C–E) NF1 or p53 expression was analyzed by immunohistochemistry (C and D) or co-immunofluorescence (E) using three different human PDAC TMAs. Representative pictures of normal areas, PanINs, and PDAC lesions are shown. Scale bars: 25 μm. The data shown in (D) represent the mean ± SEM of the percentage of overlapping samples with high or low levels of NF1 and p53 expression in the three TMAs (n = 3). The chi-square test was used to test the independence of the samples.

(F) Expression of *NF1* mRNA was analyzed by qRT-PCR using 3-month-old mice with the genotypes highlighted by the scheme (top). Mice were analyzed 4 weeks following treatment with vehicle or tamoxifen (Tam) (bottom). Data are expressed as the mean ± SEM (n = 6; 3 females and 3 males).

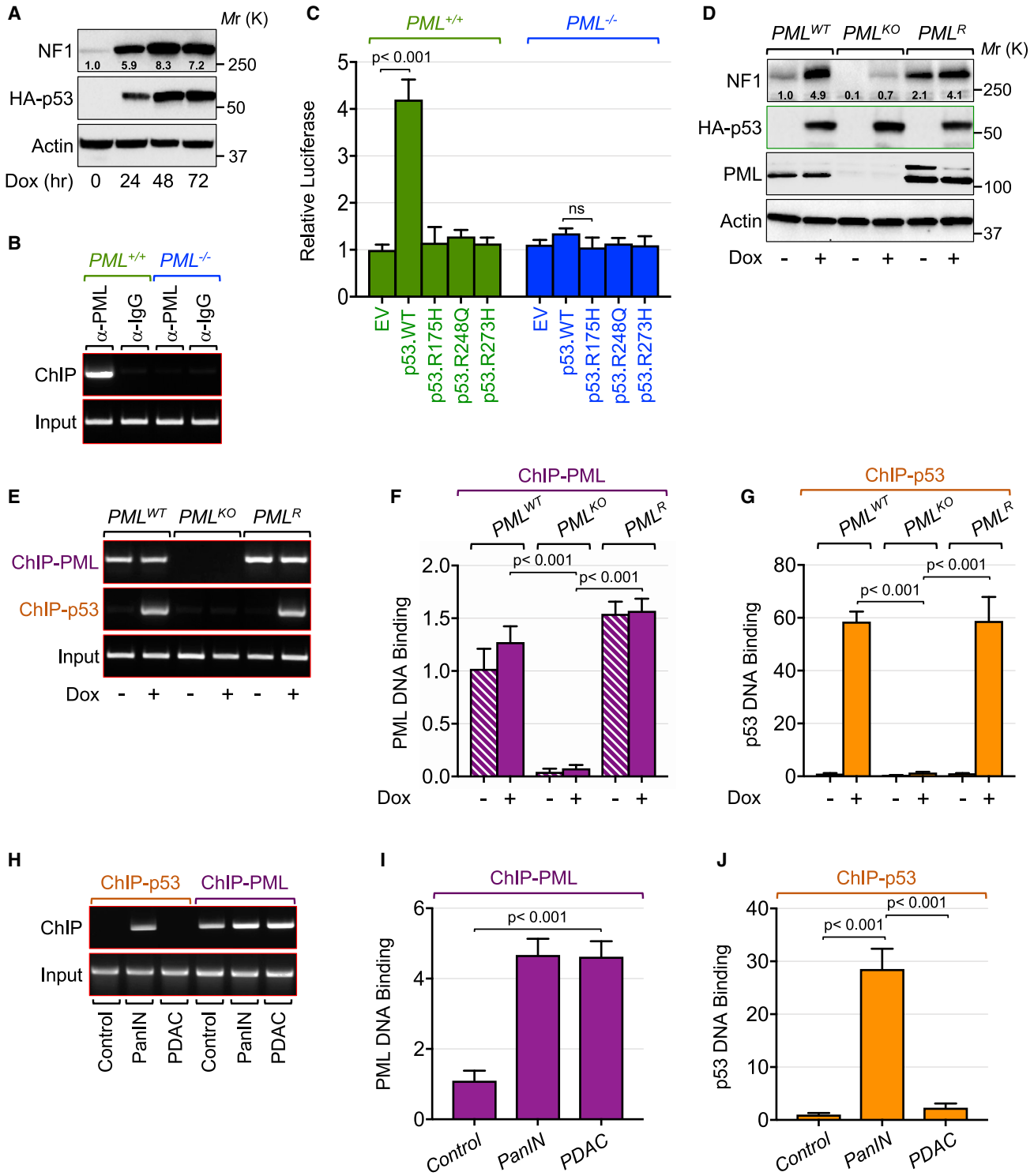

Figure 6. p53 regulates *NF1* gene expression

(A) MIA PaCa-2-Dox-HA-p53 cells were treated with Dox for the indicated times and analyzed for NF1 and HA-p53 expression by immunoblotting.

(B) MEFs from *PML*$^{+/+}$ or *PML*$^{-/-}$ mice were analyzed for the binding of PML to the *NF1* promoter by ChIP and agarose gel.

(C) MEFs from *PML*$^{+/+}$ or *PML*$^{-/-}$ mice were transfected with the NF1^{Luc} reporter in the absence or presence of p53 mutants and analyzed for luciferase activity (n = 6).

(legend continued on next page)

6G). Finally, comparative ChIP experiments using *KC* mice showed a significant increase in the binding of PML to the *NF1* promoter in mice with PanINs and full-blown PDAC (Figures 6H and 6I). More importantly, we detected a marked increase in the binding of p53 to the *NF1* promoter in tissues with PanINs, but this binding was almost lost in mice with full-blown PDAC (Figures 6H and 6J), which likely occurred owing to the decline in p53 expression typically seen at late stages of PDAC (Figure S5D). The collective observations support the conclusion that p53 functions in partnership with PML to regulate NF1 expression during PDAC progression.

Concurrent ablation of *NF1* and *p53* is sufficient to drive invasive PDAC

Having shown an association between NF1 and p53 in PDAC, we next sought to explore the consequences of their concomitant inactivation on disease development and progression. Notably, both *NF1* and *p53* alleles reside on chromosome 11 with a genetic distance of less than 4 cM, rendering the classical genetic approaches for generating sufficient numbers of double-knockout mice quite challenging because of the relatively low crossing-over recombination (~3% in our mice). To overcome this limitation, we took advantage of the mosaic analysis with double-markers (MADM) system, which enables the production of mutant cells with homozygous deletion of one or several genes residing on the same chromosome using heterozygous animals.[43] We used mice harboring heterozygous deletions of both *NF1* and *p53* together with a MADM cassette knocked into the *Hipp11* locus on chromosome 11, which is a prerequisite for using the MADM system (Figure 7A). To activate the MADM system in the pancreatic epithelium, we crossed MADM mice with *Pdx1-Cre* mice. In principle, Cre-recombinase expression is anticipated to generate a small number of mutant cells carrying homozygous deletions of both *NF1* and *p53* that are permanently labeled with GFP (green) and their sibling wild-type cells that are permanently labeled with TdTomato (red) within an otherwise colorless heterozygous pancreas (Figure 7A), a configuration that mimics the loss of heterozygosity in humans. This single-cell resolution afforded by the sparse labeling enabled one to track the mutant green cells throughout the entire process of carcinogenesis, with red sibling wild-type cells serving as internal controls. Furthermore, because mutant green and wild-type red sibling cells originate from the same mother cells in equal numbers initially, the ratio of green to red cell numbers (G/R ratio) allows for quantitative evaluation of the extent of mutant cell expansion relative to wild-type cells during the course of carcinogenesis.[43]

Similar to our prior observation, ablating *NF1* alone resulted in the formation of ADM lesions that failed to progress to PDAC (Figure S7A). We also found that ablating *p53* alone had no discernible effects on pancreas histology (Figure S7A), which is consistent with previous studies.[44] The absence of ADM in *MADM* mice with *p53* deletion alone was not surprising, as our earlier results showed, first, that homozygous ablation of *p53* reduced NF1 expression slightly below the decrease observed in mice with heterozygous deletion of *NF1* (Figure S5F) and, second, that heterozygous deletion of *NF1* was insufficient to drive ADM (Figure 3A). Strikingly, however, inactivating *p53* together with *NF1* completely shifted the indolent ADM lesions toward an aggressive and invasive PDAC phenotype (Figures 7B and 7C). Kaplan-Meier analysis showed a median survival for $MADM^{NF1/p53}$ mice of about 8 months, whereas none of the *MADM* mice with individual inactivation of *NF1* or *p53* succumbed to PDAC during this observation period (Figures 7D and S7B). Further histopathological analyses showed massive expression of the ductal marker CK19 (Figure 7C), confirming the PDAC nature of these tumors. As anticipated, the growth advantage of green mutant cells over red wild-type cells was apparent by the progressive increase in the G/R ratio (Figures 7E and 7F). At final stages of PDAC, all tumors were composed almost exclusively of GFP+ cells (Figure 7E), indicating that these tumors originate from cells with homozygous deletion of *NF1* and *p53*, and further suggesting that this cooperative oncogenic effect might operate in a cell-autonomous manner. In keeping with this notion, concomitant deletion of *NF1* and *p53* was sufficient to confer an anchorage-independent growth phenotype to HPDE cells, a phenotype that was partially rescued by adding back NF1 or p53 (Figures S7C and S7D). A similar conclusion could be drawn from the concomitant deletion of *NF1* and *PML* instead of *p53* (Figure S7C), which is in line with the requirement of PML for p53-mediated NF1 expression. In aggregates, these *in vivo* and *in vitro* data clearly demonstrate that concurrent inactivation of *NF1* and *p53* is sufficient to initiate the malignant transformation leading to PDAC.

The dismal prognosis for human PDAC is mainly attributed to the extensive metastasis to regional and distant organs seen at the time of diagnosis.[2] Common sites of local invasion include lymph nodes and spleen, whereas distant organs include liver and lung and rare instances of colon, cerebral, or bone invasion. Beyond PDAC pathogenesis and progression, the MADM strategy provided us with a unique platform to monitor the metastatic behavior of *NF1/p53*-deficient PDAC cells by assessing for the presence of GFP+ cancer cells within anticipated sites of metastasis. We consistently observed (3 of 11 mice) massive metastases to lymph nodes and spleen as well as solitary cases of metastases to the liver, as evidenced by the infiltration of GFP+ mutant cells into the organ parenchyma and subsequently confirmed by H&E staining (Figure S7E). Collectively, these genetic experiments provide unequivocal evidence that simultaneous inactivation of *NF1* and *p53* is sufficient to drive the development of invasive PDAC with aggressive metastatic behavior.

(D–G) *PML* was deleted from MIA PaCa-2-Dox-HA-p53 cells via CRISPR-Cas9, reconstituted with a CRISPR-Cas9-resistant PML mutant, and then treated with Dox for 48 h (n = 6). Cell extracts were analyzed for NF1 and HA-p53 expression by immunoblotting (D). Chromatin was analyzed for the binding of PML and p53 to the *NF1* promoter by ChIP and agarose gel (E) or qPCR (F and G).

(H–J) Pancreatic chromatin from control or *KC* mice with early PanIN (2 months) or advanced PDAC lesions (12 months) was analyzed for the binding of PML and p53 to the *NF1* promoter by ChIP and agarose gel (H) or qPCR (I and J) (n = 6; 3 females and 3 males). Data in (C), (F), (G), (I), and (J) are expressed as the mean ± SEM.

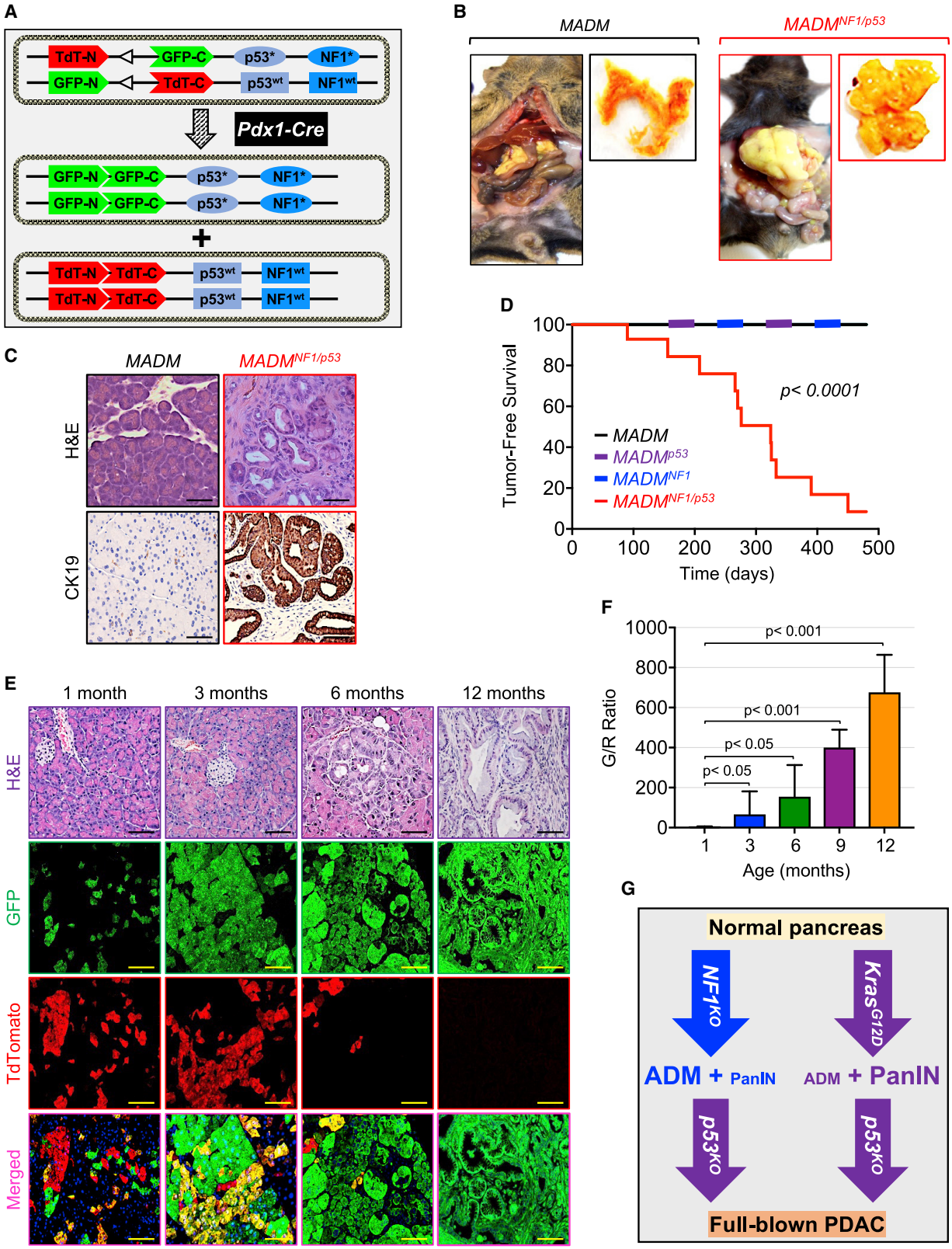

(legend on next page)

DISCUSSION

Although the current model posits that hyperactivation of Kras signaling represents an essential initiating event in PDAC, a substantial fraction of PDAC tumors harbor wild-type *KRAS*, hinting at the existence of alternative driver events. Despite intensive investigations during the past two decades, the identity of such driver events has remained elusive. Taking advantage of available clinical data from PDAC patients, we devised multiple genetic approaches to demonstrate that *NF1* inactivation plays an instrumental role in the etiology of PDAC, either functioning to facilitate PDAC progression in the presence of oncogenic $Kras^{G12D}$ or acting in concert with *p53* inactivation to initiate the development of invasive PDAC (Figure 7G). These findings have several ramifications for unraveling the enigmatic nature of the PDAC tumors that harbor wild-type *KRAS*.

Perhaps the most surprising discovery in this study was the observation that NF1 expression fluctuates significantly during PDAC progression, being relatively low to undetectable in both normal and PDAC tissues and relatively high in PanIN lesions. That transient expression of NF1 during PDAC progression is consistent with a model in which NF1 functions to orchestrate a tumor-suppressive barrier, whose disruption could be essential for full progression into the malignant state. In direct support of this notion, combining heterozygous deletion of *NF1* with $Kras^{G12D}$ resulted in a dramatic acceleration of PDAC progression in mice and anchorage-independent growth of human pancreatic cells, with the latter occurring without conferring resistance to tyrosine kinase inhibition, as these transformed cells remained addicted to EGF present in culture media. Notably, given the toxicity of the combination of $Kras^{G12D}$ and *NF1* homozygous deletion, the acquisition of oncogenic *KRAS* and homozygous inactivation of *NF1* in human PDAC might be mutually exclusive, and their simultaneous occurrence in cells might lead to their concomitant elimination. This idea could also explain why *NF1* nonsense mutations were found very rarely with mutant *KRAS* in human PDAC compared with mutations in the tumor-suppressor genes *TP53*, *p16INK4A*, and *SMAD4*, as abundant literature has shown that the latter mutations were not mutually exclusive with *KRAS* mutations in PDAC.[10–13] Also, this idea raises the provocative possibility that targeting NF1 in mutant KRAS-bearing PDAC tumors might create vulnerabilities that could be exploited for therapeutic advantage.

Intriguingly, we found that homozygous inactivation of *NF1* alone culminated in the formation of ADM and occasionally early stages PanINs, although those lesions failed to progress to PDAC even during a period exceeding 12 months, a time at which a significant fraction of mice with $Kras^{G12D}$ alone succumbed to PDAC.[8,27] Although these findings imply that *NF1* inactivation might not be sufficient to drive PDAC in a wild-type *Kras* background, it did not rule out the possibility that *NF1* inactivation might render pancreatic cells sensitive to other genetic alterations that occur frequently in human PDAC, such as mutational inactivation of *p53*.[36] In efforts to probe this possibility, we conducted genetic experiments using MADM, an elegant and powerful approach that not only eliminates variations that are invariably introduced by comparing phenotypes between individual animals but also allows for differential labeling of both normal (TdTomato) and cancer (GFP) cells, thereby facilitating analysis of cancer evolution and its spread to distant organs.[43] Exploiting the MADM system in the context of PDAC, we demonstrated that concomitant inactivation of *NF1* and *p53* was sufficient to drive full-blown PDAC. At necropsy, we detected tumor masses displaying almost exclusively GFP fluorescence, clearly indicating that these tumors were originating initially from cells with *NF1* and *p53* deleted. Moreover, these tumors displayed the characteristic features of PDAC, as evidenced by the abundance of PanIN lesions that exhibited high reactivity to the CK19 antibody as well as the dissemination of GFP+ mutant cells to both local and distant sites associated with human PDAC.[2] Of note, *NF1* deletion alone resulted in the formation of benign ADMs and eventually early stage PanINs that failed to progress to PDAC. In contrast, inactivating *p53* alone had no discernible effect on pancreas histology, suggesting that *NF1* inactivation, rather than *p53* inactivation, might represent the initiating event leading to PDAC in $MADM^{NF1/p53}$ mice.

Another fascinating observation was the strong association between NF1 and p53 in PDAC. For instance, we noticed a transient expression of p53 during human PDAC progression, mirroring the transient expression seen for NF1. Such association between NF1 and p53 expression is not restricted to human PDAC, as we observed a similar pattern in three different GEMMs of PDAC. Mechanistically, we provided evidence that p53 is recruited to the *NF1* promoter through its association with PML, which is known to mediate key p53 tumor-suppressor functions, such as senescence, cell-cycle arrest, and apoptosis.[41,42] While a decisive conclusion regarding the exact contribution of PML to PDAC is still awaiting further *in vivo* experimental validation using GEMMs, our malignant transformation assays using HPDE cells raise the possibility that PML might function as an auxiliary component of the NF1/p53 tumor-suppressor network that operates transiently to restrict PDAC progression. In addition to PML, because we found that a substantial fraction of human PDAC samples also harbor mutations in *p16INK4A* and

Figure 7. Concurrent ablation of *NF1* and *p53* culminates in PDAC formation and progression

(A) Schematic model of $MADM^{NF1/p53}$ conditional activation in pancreas.

(B) Representative pictures of 10-month-old *MADM* and $MADM^{NF1/p53}$ mice (female and male) and their corresponding pancreas when $MADM^{NF1/p53}$ mice developed invasive PDAC.

(C) FFPE pancreatic tissues from 10-month-old mice with the indicated genotypes were analyzed by H&E or immunohistochemistry using anti-CK19 antibody. Representative pictures are shown (n = 7–16; 3–9 females and 4–7 males). Scale bars: 25 μm.

(D) Kaplan-Meier analysis of survival of mice with the indicated genotypes (n = 16; 7–9 females and 7–9 males).

(E and F) FFPE pancreatic tissues from $MADM^{NF1/p53}$ mice at different ages (1–12 months) were subjected to H&E or DAPI staining and analyzed for GFP (green), TdTomato (red), and nuclei (blue). Representative pictures are shown. Scale bars: 50 μm (E). The green/red (G/R) ratio was determined by quantifying all cells in the section (F). Data are expressed as the mean ± SEM (n = 12; 6 females and 6 males).

(G) Model depicting how NF1 interacts with Kras or p53 to influence PDAC pathogenesis and progression.

SMAD4, it would be interesting to determine in future genetic studies whether simultaneous inactivation of *NF1* and *p16Ink4a* or *Smad4* would be sufficient to drive PDAC, as does simultaneous inactivation of *NF1* and *p53*.

Of particular relevance, *NF1* and *p53* localize to the same chromosome in both humans and mice, which creates another layer of complexity both in terms of their expression and in terms of their mutational status. In future investigations, it would be tantalizing to explore whether *NF1* and *p53* could be subjected to the same mutational pressure that is unleashed by deleterious global genetic events, such as chromothripsis, which occurs frequently in human PDAC.[45] Because chromothripsis is deemed to provoke the pulverization of an entire chromosome with subsequent random chromosomal reconstitutions permissive for massive DNA alterations during one aberrant cell cycle,[46] one would speculate that inactivation of *NF1* and *p53* might occur simultaneously with additional genetic alterations that could activate or inactivate other oncogenes or tumor-suppressor genes within chromosome 17, respectively. Although conceivable, this scenario is likely to be incremental, as simultaneous deletion of *NF1* and *p53* was sufficient to drive PDAC pathogenesis and progression in mice. In closing, the notion that concurrent inactivation of *NF1* and p53 represents an alternative initiating event in PDAC provides an unprecedented platform for future identification of potential targets amenable to therapeutic intervention in PDAC with wild-type *KRAS*, and possibly in other malignancies with similar genetic alterations.

Limitations of the study

Our extensive analysis of available public datasets revealed the presence of various coding mutations within the *NF1* locus in a significant proportion of human PDAC tumors. Due to the large number of mutations identified, we were not able to conduct a comprehensive characterization of the different mutations on NF1 protein function. While nonsense mutations or frameshifts created by insertions, deletions, or splice junction mutations can result in the loss of protein expression, the functional consequence of missense mutations on NF1 Ras-GAP activity was not explored in this study. Another limitation pertains to the association between p53 and NF1. While the effect of inactivating mutations in *p53* on NF1 expression was demonstrated, the reciprocal consequence of *NF1*-inactivating mutations on p53 expression warrants future investigation. Finally, it also remains to be explored whether *NF1* inactivation could cooperate with inactivating mutations in *p16Ink4A* or *Smad4* to drive PDAC pathogenesis and progression, as does in the context of *p53* inactivation.

STAR★METHODS

Detailed methods are provided in the online version of this paper and include the following:

- KEY RESOURCES TABLE
- RESOURCE AVAILABILITY
  - Lead contact
  - Materials availability
  - Data and code availability
- EXPERIMENTAL MODEL AND SUBJECT DETAILS
  - Mice
  - Clinical samples
  - Cell lines
- METHOD DETAILS
  - Plasmid constructs
  - Mice treatment and analysis
  - Cell lines and culture
  - Soft agar colony formation assay
  - Ras-GTP pulldown assay
  - Immunoblotting
  - Immunofluorescence and immunohistochemistry
  - Real-time PCR (RT-PCR)
  - Chromatin immunoprecipitation assay (ChIP)
  - Luciferase reporter assay
  - Analysis of public datasets
- QUANTIFICATION AND STATISTICAL ANALYSIS

SUPPLEMENTAL INFORMATION

Supplemental information can be found online at https://doi.org/10.1016/j.celrep.2022.111623.

ACKNOWLEDGMENTS

We thank Dr. N. Sharpless for providing *p16Inkk4a*^{Luc} mice, Dr. P. Pandolfi for providing *PML*$^{+/+}$ and *PML*$^{-/-}$ MEFs, and Dr. L. Martinez for providing p53 constructs. We thank Drs. P. Howe, P. Bos, and K. Kordula for their critical reading of the manuscript. This work was supported by grants from the NIH/NCI (R01CA210911, R01CA240484, and R01CA251405) to A.A.

AUTHOR CONTRIBUTIONS

G.R. and P.P. were responsible for the experimental design and data analysis. P.S. was responsible for mouse breeding, genotyping, and pancreas preparation. A.A., P.S., and C.P. contributed to the molecular and biochemical experiments. G.R., C.P., and A.A. generated molecular and biological tools. C.F., E.H., M.S.R., and K.X. contributed to pancreas histology experiments and dataset analysis. A.A., K.X., and M.S.R. wrote the manuscript with input from all other authors.

DECLARATION OF INTERESTS

The authors declare no competing interests.

Received: December 13, 2021
Revised: July 21, 2022
Accepted: October 18, 2022
Published: November 8, 2022

REFERENCES

1. Siegel, R.L., Miller, K.D., and Jemal, A. (2020). Cancer statistics, 2020. CA. Cancer J. Clin. *70*, 7–30.
2. Mizrahi, J.D., Surana, R., Valle, J.W., and Shroff, R.T. (2020). Pancreatic cancer. Lancet *395*, 2008–2020.
3. Stathis, A., and Moore, M.J. (2010). Advanced pancreatic carcinoma: current treatment and future challenges. Nat. Rev. Clin. Oncol. *7*, 163–172.
4. Almoguera, C., Shibata, D., Forrester, K., Martin, J., Arnheim, N., and Perucho, M. (1988). Most human carcinomas of the exocrine pancreas contain mutant c-K-ras genes. Cell *53*, 549–554.

5. Hezel, A.F., Kimmelman, A.C., Stanger, B.Z., Bardeesy, N., and Depinho, R.A. (2006). Genetics and biology of pancreatic ductal adenocarcinoma. Genes Dev. *20*, 1218–1249.
6. Iacobuzio-Donahue, C.A. (2012). Genetic evolution of pancreatic cancer: lessons learnt from the pancreatic cancer genome sequencing project. Gut *61*, 1085–1094.
7. Bailey, P., Chang, D.K., Nones, K., Johns, A.L., Patch, A.M., Gingras, M.C., Miller, D.K., Christ, A.N., Bruxner, T.J.C., Quinn, M.C., et al. (2016). Genomic analyses identify molecular subtypes of pancreatic cancer. Nature *531*, 47–52.
8. Hingorani, S.R., Petricoin, E.F., Maitra, A., Rajapakse, V., King, C., Jacobetz, M.A., Ross, S., Conrads, T.P., Veenstra, T.D., Hitt, B.A., et al. (2003). Preinvasive and invasive ductal pancreatic cancer and its early detection in the mouse. Cancer Cell *4*, 437–450.
9. Tuveson, D.A., Shaw, A.T., Willis, N.A., Silver, D.P., Jackson, E.L., Chang, S., Mercer, K.L., Grochow, R., Hock, H., Crowley, D., et al. (2004). Endogenous oncogenic K-ras(G12D) stimulates proliferation and widespread neoplastic and developmental defects. Cancer Cell *5*, 375–387.
10. Bardeesy, N., Aguirre, A.J., Chu, G.C., Cheng, K.H., Lopez, L.V., Hezel, A.F., Feng, B., Brennan, C., Weissleder, R., Mahmood, U., et al. (2006). Both p16(Ink4a) and the p19(Arf)-p53 pathway constrain progression of pancreatic adenocarcinoma in the mouse. Proc. Natl. Acad. Sci. USA *103*, 5947–5952.
11. Bardeesy, N., Cheng, K.H., Berger, J.H., Chu, G.C., Pahler, J., Olson, P., Hezel, A.F., Horner, J., Lauwers, G.Y., Hanahan, D., and DePinho, R.A. (2006). Smad4 is dispensable for normal pancreas development yet critical in progression and tumor biology of pancreas cancer. Genes Dev. *20*, 3130–3146.
12. Aguirre, A.J., Bardeesy, N., Sinha, M., Lopez, L., Tuveson, D.A., Horner, J., Redston, M.S., and DePinho, R.A. (2003). Activated Kras and Ink4a/Arf deficiency cooperate to produce metastatic pancreatic ductal adenocarcinoma. Genes Dev. *17*, 3112–3126.
13. Hingorani, S.R., Wang, L., Multani, A.S., Combs, C., Deramaudt, T.B., Hruban, R.H., Rustgi, A.K., Chang, S., and Tuveson, D.A. (2005). Trp53R172H and KrasG12D cooperate to promote chromosomal instability and widely metastatic pancreatic ductal adenocarcinoma in mice. Cancer Cell *7*, 469–483.
14. Tsuchida, N., Ryder, T., and Ohtsubo, E. (1982). Nucleotide sequence of the oncogene encoding the p21 transforming protein of Kirsten murine sarcoma virus. Science *217*, 937–939.
15. Scheffzek, K., Ahmadian, M.R., Kabsch, W., Wiesmüller, L., Lautwein, A., Schmitz, F., and Wittinghofer, A. (1997). The Ras-RasGAP complex: structural basis for GTPase activation and its loss in oncogenic Ras mutants. Science *277*, 333–338.
16. Hennig, A., Markwart, R., Esparza-Franco, M.A., Ladds, G., and Rubio, I. (2015). Ras activation revisited: role of GEF and GAP systems. Biol. Chem. *396*, 831–848.
17. Hobbs, G.A., Der, C.J., and Rossman, K.L. (2016). RAS isoforms and mutations in cancer at a glance. J. Cell Sci. *129*, 1287–1292.
18. Ihle, N.T., Byers, L.A., Kim, E.S., Saintigny, P., Lee, J.J., Blumenschein, G.R., Tsao, A., Liu, S., Larsen, J.E., Wang, J., et al. (2012). Effect of KRAS oncogene substitutions on protein behavior: implications for signaling and clinical outcome. J. Natl. Cancer Inst. *104*, 228–239.
19. Adari, H., Lowy, D.R., Willumsen, B.M., Der, C.J., and McCormick, F. (1988). Guanosine triphosphatase activating protein (GAP) interacts with the p21 ras effector binding domain. Science *240*, 518–521.
20. Lito, P., Solomon, M., Li, L.S., Hansen, R., and Rosen, N. (2016). Allele-specific inhibitors inactivate mutant KRAS G12C by a trapping mechanism. Science *351*, 604–608.
21. Stalnecker, C.A., and Der, C.J. (2020). RAS, wanted dead or alive: advances in targeting RAS mutant cancers. Sci. Signal. *13*, eaay6013.
22. Xu, G.F., O'Connell, P., Viskochil, D., Cawthon, R., Robertson, M., Culver, M., Dunn, D., Stevens, J., Gesteland, R., White, R., et al. (1990). The neurofibromatosis type 1 gene encodes a protein related to GAP. Cell *62*, 599–608.
23. Martin, G.A., Viskochil, D., Bollag, G., McCabe, P.C., Crosier, W.J., Haubruck, H., Conroy, L., Clark, R., O'Connell, P., Cawthon, R.M., et al. (1990). The GAP-related domain of the neurofibromatosis type 1 gene product interacts with ras p21. Cell *63*, 843–849.
24. Ratner, N., and Miller, S.J. (2015). A RASopathy gene commonly mutated in cancer: the neurofibromatosis type 1 tumour suppressor. Nat. Rev. Cancer *15*, 290–301.
25. Mazur, P.K., and Siveke, J.T. (2012). Genetically engineered mouse models of pancreatic cancer: unravelling tumour biology and progressing translational oncology. Gut *61*, 1488–1500.
26. Parajuli, P., Nguyen, T.L., Prunier, C., Razzaque, M.S., Xu, K., and Atfi, A. (2020). Pancreatic cancer triggers diabetes through TGF-beta-mediated selective depletion of islet beta-cells. Life Sci. Alliance *3*, e201900573.
27. Parajuli, P., Singh, P., Wang, Z., Li, L., Eragamreddi, S., Ozkan, S., Ferrigno, O., Prunier, C., Razzaque, M.S., Xu, K., and Atfi, A. (2019). TGIF1 functions as a tumor suppressor in pancreatic ductal adenocarcinoma. EMBO J. *38*, e101067.
28. Gu, G., Brown, J.R., and Melton, D.A. (2003). Direct lineage tracing reveals the ontogeny of pancreatic cell fates during mouse embryogenesis. Mech. Dev. *120*, 35–43.
29. Storz, P. (2017). Acinar cell plasticity and development of pancreatic ductal adenocarcinoma. Nat. Rev. Gastroenterol. Hepatol. *14*, 296–304.
30. Kopp, J.L., von Figura, G., Mayes, E., Liu, F.F., Dubois, C.L., Morris, J.P., 4th, Pan, F.C., Akiyama, H., Wright, C.V.E., Jensen, K., et al. (2012). Identification of Sox9-dependent acinar-to-ductal reprogramming as the principal mechanism for initiation of pancreatic ductal adenocarcinoma. Cancer Cell *22*, 737–750.
31. Guerra, C., Schuhmacher, A.J., Cañamero, M., Grippo, P.J., Verdaguer, L., Pérez-Gallego, L., Dubus, P., Sandgren, E.P., and Barbacid, M. (2007). Chronic pancreatitis is essential for induction of pancreatic ductal adenocarcinoma by K-Ras oncogenes in adult mice. Cancer Cell *11*, 291–302.
32. Lerch, M.M., and Gorelick, F.S. (2013). Models of acute and chronic pancreatitis. Gastroenterology *144*, 1180–1193.
33. Burd, C.E., Sorrentino, J.A., Clark, K.S., Darr, D.B., Krishnamurthy, J., Deal, A.M., Bardeesy, N., Castrillon, D.H., Beach, D.H., and Sharpless, N.E. (2013). Monitoring tumorigenesis and senescence in vivo with a p16(INK4a)-luciferase model. Cell *152*, 340–351.
34. Deer, E.L., González-Hernández, J., Coursen, J.D., Shea, J.E., Ngatia, J., Scaife, C.L., Firpo, M.A., and Mulvihill, S.J. (2010). Phenotype and genotype of pancreatic cancer cell lines. Pancreas *39*, 425–435.
35. Leung, L., Radulovich, N., Zhu, C.Q., Wang, D., To, C., Ibrahimov, E., and Tsao, M.S. (2013). Loss of canonical Smad4 signaling promotes KRAS driven malignant transformation of human pancreatic duct epithelial cells and metastasis. PLoS One *8*, e84366.
36. Waddell, N., Pajic, M., Patch, A.M., Chang, D.K., Kassahn, K.S., Bailey, P., Johns, A.L., Miller, D., Nones, K., Quek, K., et al. (2015). Whole genomes redefine the mutational landscape of pancreatic cancer. Nature *518*, 495–501.
37. Muller, P.A.J., and Vousden, K.H. (2014). Mutant p53 in cancer: new functions and therapeutic opportunities. Cancer Cell *25*, 304–317.
38. Lavin, M.F., and Gueven, N. (2006). The complexity of p53 stabilization and activation. Cell Death Differ. *13*, 941–950.
39. Ventura, A., Kirsch, D.G., McLaughlin, M.E., Tuveson, D.A., Grimm, J., Lintault, L., Newman, J., Reczek, E.E., Weissleder, R., and Jacks, T. (2007). Restoration of p53 function leads to tumour regression in vivo. Nature *445*, 661–665.
40. el-Deiry, W.S., Kern, S.E., Pietenpol, J.A., Kinzler, K.W., and Vogelstein, B. (1992). Definition of a consensus binding site for p53. Nat. Genet. *1*, 45–49.

41. de Stanchina, E., Querido, E., Narita, M., Davuluri, R.V., Pandolfi, P.P., Ferbeyre, G., and Lowe, S.W. (2004). PML is a direct p53 target that modulates p53 effector functions. Mol. Cell *13*, 523–535.

42. Ferbeyre, G., de Stanchina, E., Querido, E., Baptiste, N., Prives, C., and Lowe, S.W. (2000). PML is induced by oncogenic ras and promotes premature senescence. Genes Dev. *14*, 2015–2027.

43. Liu, C., Sage, J.C., Miller, M.R., Verhaak, R.G.W., Hippenmeyer, S., Vogel, H., Foreman, O., Bronson, R.T., Nishiyama, A., Luo, L., and Zong, H. (2011). Mosaic analysis with double markers reveals tumor cell of origin in glioma. Cell *146*, 209–221.

44. Muzumdar, M.D., Dorans, K.J., Chung, K.M., Robbins, R., Tammela, T., Gocheva, V., Li, C.M.C., and Jacks, T. (2016). Clonal dynamics following p53 loss of heterozygosity in Kras-driven cancers. Nat. Commun. *7*, 12685.

45. Notta, F., Chan-Seng-Yue, M., Lemire, M., Li, Y., Wilson, G.W., Connor, A.A., Denroche, R.E., Liang, S.B., Brown, A.M.K., Kim, J.C., et al. (2016). A renewed model of pancreatic cancer evolution based on genomic rearrangement patterns. Nature *538*, 378–382.

46. Korbel, J.O., and Campbell, P.J. (2013). Criteria for inference of chromothripsis in cancer genomes. Cell *152*, 1226–1236.

47. Zhang, M.Z., Ferrigno, O., Wang, Z., Ohnishi, M., Prunier, C., Levy, L., Razzaque, M., Horne, W.C., Romero, D., Tzivion, G., et al. (2015). TGIF governs a feed-forward network that empowers Wnt signaling to drive mammary tumorigenesis. Cancer Cell *27*, 547–560.

48. Parajuli, P., Kumar, S., Loumaye, A., Singh, P., Eragamreddy, S., Nguyen, T.L., Ozkan, S., Razzaque, M.S., Prunier, C., Thissen, J.P., and Atfi, A. (2018). Twist1 activation in muscle progenitor cells causes muscle loss akin to cancer cachexia. Dev. Cell *45*, 712–725.e6.

49. Lin, H.K., Bergmann, S., and Pandolfi, P.P. (2004). Cytoplasmic PML function in TGF-beta signalling. Nature *431*, 205–211.

STAR★METHODS

KEY RESOURCES TABLE

REAGENT or RESOURCE	SOURCE	IDENTIFIER
Antibodies		
Kras	Abcam	ab275876
Hras	Abcam	Cat# ab32417; RRID:AB_726959
Kras	Santa Cruz Bio.	Cat# sc-30; RRID:AB_627865
Nras	Abcam	Cat# ab300431;
Nras	Abcam	Cat# Ab77392; RRID:AB_1524048
Ras	Cell Signaling	Cat# 67648; RRID:AB_2910195
NF1	Cell Signaling	Cat# 14623; RRID:AB_2798543
NF1	Abcam	Cat# ab17963; RRID:AB_444142
NF1	Santa Cruz Bio.	Cat# sc-20017; RRID:AB_628008
ERK	Cell Signaling	Cat# 4695; RRID:AB_390779
pERK	Cell Signaling	Cat# 3510; RRID:AB_1595393
AKT	Cell Signaling	Cat# 4691; RRID:AB_915783
pAKT	Cell Signaling	Cat# 4060; RRID:AB_2315049
Cytokeratin 19	Abcam	Cat# Ab15463; RRID:AB_2281021
Muc5AC	Abcam	Cat# Ab3649; RRID:AB_2146844
Sox9	Cell Signaling	Cat# 82630; RRID:AB_2665492
p53	Santa Cruz Bio.	Cat# Sc-126; RRID:AB_628082
p53	Millipore Sigma	SAB5700817
PML	Santa Cruz Bio.	Cat# Sc-966; RRID:AB_628162
PML	Santa Cruz Bio.	Cat#; sc-377390; RRID:AB_2910213
PML	Millipore Sigma	MAB3738
Insulin	Cell Signaling	Cat# 3014; RRID:AB_2126503
Glucagon	Cell Signaling	Cat# 8233; RRID:AB_10859908
GAPDH	Cell Signaling	Cat # 5174; RRID:AB_10622025
Goat anti-rabbit Alexa-Fluor®568	Invitrogen	A11011
Goat anti-rabbit Alexa-Fluor®488	Invitrogen	A11008
Goat anti-rabbit HRP	Cell Signaling	Cat# 7074S; RRID:AB_2099233
Goat anti-mouse HRP	Cell Signaling	Cat# 7076S; RRID:AB_330924
HA	Millipore Sigma	11867423001
β-Actin	Abcam	Cat# Ab6276; RRID:AB_2223210
Chemicals, peptides, and recombinant proteins		
D-luciferin	Perkin Elmer	122799
Doxycycline	Sigma-Aldrich	F3685
Puromycin	Sigma-Aldrich	P9620
G418	Sigma-Aldrich	4727878001
Hygromycin B	Sigma-Aldrich	10843555001
Blasticidin	ThermoFisher	A1113903
Caerulein	Sigma-Aldrich	C9026
EGF	Gibco	10450-013
bovine pituitary extract	Gibco	13028-014
Keratinocyte SFM media	Gibco	10724-011
Agar	Sigma-Aldrich	A1296
X-tremeGENE9	Millipore Sigma	6365779001

(*Continued on next page*)

Continued

REAGENT or RESOURCE	SOURCE	IDENTIFIER
Critical commercial assays		
VECTASTAN Elite ABC HRP kit	Vector Laboratories	PK-6100
DAB Peroxidase Substrate Kit	Vector Laboratories	SK-4100
In-Fusion® HD Cloning Plus	Takara	638920
MTT assays kit	Abcam	Ab211091
Active Ras Detection Kit	Cell Signaling	8821
Chromatin Immunoprecipitation Assay kit	Millipore	17-295
Dual-Luciferase Reporter Assay kit	Promega	E1910
In-Fusion HD Cloning Plus Kit	Takara	638920
QuickChange Site-Directed Mutagenesis	Agilent	200521
Platinum SuperFi II DNA Polymerase–High-Fidelity	ThermoFisher	12361010
Lenti-X Packaging Single Shots	Takara	631282
Recombinant DNA		
pLVX-Tet3G	Takara	631187
pLVX-Tre3G	Takara	631187
pLVX-Tre3G-HA-p53	This study	N/A
pLVX-Tre3G-HA-p53.R248Q	This study	N/A
pLVX-Tre3G-HA-p53.R273H	This study	N/A
pLVX-Tre3G-NF1	This study	N/A
pLVX-IRES-Neo-NF1^{R}	This study	N/A
pLVX-IRES-Neo-p53^{R}	This study	N/A
pCMV5-HA-PML-IV	This study	N/A
pQCXIP-p53	Dr. Martinez	UMMC
pQCXIP-p53.R248Q	Dr. Martinez	UMMC
pQCXIP-p53.R273H	Dr. Martinez	UMMC
pQCXIP-p53.R172H	Dr. Martinez	UMMC
pBABE-HA-Kras^{G12D}	Addgene	58902
pBABE-HA-Kras^{G12C}	Addgene	58901
pCMV5-HA-PML	This study	N/A
pLVX-Hyg-PML^{R}	This study	N/A
pGL3-NF1^{Luc} (all mutants)	This study	N/A
pRL-SV40	Promega	E2231
pGL3-Basic	Promega	PR-E1751
pCMV-VSV-G	Addgene	8454
pUMVC	Addgene	8449
Flag-PML IV/pRK5	Addgene	59742
pLVX-IRES-Hyg-Smad4	Addgene	107128
pLVX-IRES-Neo	Takara	632181
pCMV5B-2xHA	Wrana J.	Zhang et al., 2015, Parajuli et al., 2018[47, 48]
LentiCRISPRv2-blast	Addgene	98293
LentiCRISPRv2	Addgene	52961
LentiCRISPRv2-Kras-gRNAs	GenScript	SC1805
LentiCRISPRv2-NF1-gRNA	GenScript	SC1678
LentiCRISPRv2-p53-gRNA	GenScript	SC1805
LentiCRISPRv2-PML-gRNA	GenScript	SC1805

(*Continued on next page*)

Continued		
REAGENT or RESOURCE	SOURCE	IDENTIFIER
Experimental models: Cell lines		
Panc-1	ATCC	CRL-1469
Panc-1-Dox-HA-p53	This study	N/A
MIA PaCa-2	ATCC	CRL-1420
MIA PaCa-2-Dox-HA-p53	This study	N/A
MIA PaCa-2-Dox-HA-p53-PML^{KO}	This study	N/A
MIA PaCa-2-Dox-HA-p53.R248K	This study	N/A
MIA PaCa-2-Dox-HA-p53.R273H	This study	N/A
MIA PaCa-2-Dox-HA-p53-PML^{R}	This study	N/A
MIA PaCa-2-Dox-NF1	This study	N/A
MIA PaCa-2-Dox-NF1-HA-Kras^{G12C}	This study	N/A
HPDE	Kerafast	ECA001-FP
HPDE-HA-Kras^{G12D}	This study	N/A
HPDE-NF1^{KO}	This study	N/A
HPDE-HA-Kras^{G12D}-NF1^{KO}	This study	N/A
HPDE-HA-Kras^{G12D}-NF1^{KO}-NF1^{R}	This study	N/A
HPDE-NF1^{KO}-p53^{KO}	This study	N/A
HPDE-NF1^{KO}-p53^{KO}-NF1^{R}	This study	N/A
HPDE-NF1^{KO}-p53^{KO}-p53^{R}	This study	N/A
HPDE-NF1^{KO}-PML^{KO}	This study	N/A
HEK293T	ATCC	CRL-2638
PML$^{-/-}$ MEFs	Dr. Pandolfi	Lin et al., 2004[49]
PML$^{+/+}$ MEFs	Dr. Pandolfi	Lin et al., 2004[49]
Experimental models: Organisms/strains		
Loxp-Stop-Loxp-Kras^{G12D}	NCI	01XJ6
p16Ink4a^{Luc}	Dr. Sharpless	Burd et al., 2013[33]
Pdx1-Cre	NCI	01XL5
Pdx1-Cre^{ERT2}	Jackson Lab.	024968
MADM^{TG}-p53$^{+/-}$NF1$^{fl/+}$	Jackson Lab.	017530
MADM^{TG}-p53$^{+/-}$	This study	N/A
MADM^{TG}-NF1$^{fl/+}$	This study	N/A
NF1$^{fl/fl}$	This study	N/A
MADM^{GT}	Jackson Lab.	013749
Trp53$^{fl/fl}$	Jackson Lab.	008462
LSL-Trp53	Jackson Lab.	008361
Smad4$^{fl/fl}$	Jackson Lab.	017462

RESOURCE AVAILABILITY

Lead contact

Further information and requests for resources and reagents should be directed to and will be fulfilled by the lead contact, Azeddine Atfi (azeddine.atfi@inserm.fr or azeddine.atfi@vcuhealth.org).

Materials availability

All unique reagents generated during this study are available from the lead contact without restriction.

Data and code availability

- All data reported in this paper will be shared by the lead contact upon request.
- This paper does not report original code.
- Any additional information required to reanalyze the data reported in this paper is available from the lead contact upon request.

EXPERIMENTAL MODEL AND SUBJECT DETAILS

Mice

MADM^{TG};*p53*$^{+/-}$;*NF1*$^{fl/+}$, *MADM*^{GT}, *Smad4*$^{fl/fl}$, *Trp53*$^{fl/fl}$, *LSL-Trp53* and *Pdx1-Cre*^{ERT2} mice were obtained from Jackson Laboratories. *Loxp-Stop-Loxp-Kras*^{G12D} (*Kras*^{G12D}) and *Pdx1-Cre* mice were obtained from the NCI Mouse Repository. *p16Ink4a*^{Luc} (*p16*^{Luc}) was kindly provided by Dr. Sharpless.[33] To generate mice with pancreas-specific homozygous deletion of *NF1* (*NF1*^{KO}), *MADM*^{TG}-*p53*$^{+/-}$*NF1*$^{fl/+}$ mice were first interbred to obtain pure *NF1*$^{fl/fl}$ mice without the MADM cassette as well as the *p53* heterozygous allele and then the resulting *NF1*$^{fl/fl}$ mice were crossbred with *Pdx1-Cre* mice. To generate *MADM*$^{NF1/p53}$ mice, *MADM*^{TG}-*p53*$^{+/-}$*NF1*$^{fl/+}$ mice (homozygous for *MADM* and heterozygous for both *NF1* and *p53*) were crossbreed with mice harboring homozygous *MADM*^{GT} cassette and *Pdx1-Cre*. To generate *MADM*^{NF1} mice, *MADM*^{TG}-*NF1*$^{fl/+}$ mice (homozygous for *MADM* and heterozygous for *NF1*) were crossbred with mice harboring homozygous *MADM*^{GT} cassette and *Pdx1-Cre*. To generate *MADM*^{p53} mice, *MADM*^{TG}-*p53*$^{+/-}$ mice (homozygous for *MADM* and heterozygous for *p53*) were crossbred with mice harboring homozygous *MADM*^{GT} cassette and *Pdx1-Cre*. The other PDAC mouse models were generated through successive crossbreeding of *Pdx1-Cre*, *Pdx1-Cre*^{ERT2}, *LSL-Kras*^{G12D}, *Trp53*$^{fl/fl}$, *Smad4*$^{fl/fl}$, *LSL-Trp53* and *p16*^{Luc} mice using classical approaches.[26,27] Full descriptions of the genotypes of mice used throughout the study are:

-NF1^{KO} = NF1$^{fl/fl}$;Pdx1-Cre
-NC= NF1$^{fl/+}$;Pdx1-Cre
-KC= LSL-Kras^{G12D};Pdx1-Cre
-KNC= LSL-Kras^{G12D};NF1$^{fl/+}$;Pdx1-Cre
-KPC= LSL-Kras^{G12D}*;Trp53*$^{fl/fl}$*;Pdx1-Cre*
-p53^{KO}= Trp53$^{fl/fl}$;Pdx1-Cre
-KrPC^{Tam}= LSL-Kras^{G12D};LSL-Trp53;Pdx1-Cre^{ERT2}
-KPC^{Tam}= LSL-Kras^{G12D};Trp53$^{fl/fl}$;Pdx1-Cre^{ERT2}
-KSC= LSL-Kras^{G12D}*;Smad4*$^{fl/fl}$*;Pdx1-Cre*
-KIC= LSL-Kras^{G12D};p16$^{Luc+/+}$;Pdx1-Cre
-KI^{Luc}C= LSL-Kras^{G12D};p16$^{Luc+/-}$;Pdx1-Cre
-NI^{Luc}C= NF1$^{fl/+}$;p16$^{Luc+/-}$;Pdx1-Cre
-KNI^{Luc}C= LSL-Kras^{G12D};NF1$^{fl/+}$;p16$^{Luc+/-}$;Pdx1-Cre
-I^{Luc}= p16$^{Luc+/-}$;Pdx1-Cre
-MADM= MADM^{TG};MADM^{GT};Pdx1-Cre
-MADM^{NF1}= MADM^{TG}-NF1$^{fl/+}$;MADM^{GT};Pdx1-Cre
-MADM^{p53}= MADM^{TG}-p53$^{+/-}$;MADM^{GT};Pdx1-Cre
-MADM$^{NF1/p53}$= MADM^{TG}-p53$^{+/-}$-NF1$^{fl/+}$;MADM^{GT};Pdx1-Cre

All mice were maintained on a mixed C57BL/6 and FVB/N genetic background. Mice were maintained in 12 h light:dark cycles (6:00 am to 6:00 pm) at 22°C and fed a standard rodent chow diet. The Institutional Animal Care and Use Committee (IACUC) of the University of Mississippi Medical Center (UMMC) or Virginia Commonwealth University approved all animal experiments.

Clinical samples

The three Human Tissue Micro Arrays for pancreatic tissues used in the study contain 80, 80 and 96, respectively. They were obtained from US Biomax Inc. Among the 256 samples, 179 were reported either as normal (65) or PDAC (114) tissues.

Cell lines

Wild-type HEK293T, MIA PaCa-2 and Panc-1 cells were obtained from the American Type Culture Collection (ATCC). HPDE cells were obtained from Kerafast. To generate MIA PaCa-2-Dox-HA-p53 and Panc-1-Dox-HA-p53 cell lines, cells were transduced with the bicistronic pLVX-Tet3G lentiviruses (Takara) and selected with G418. Pools of cells expressing the Tet-transactivator were then transduced with pLVX-Tre3G-HA-p53, pLVX-Tre3G-HA-p53.R248Q or pLVX-Tre3G-HA-p53.R273H lentiviruses, selected with puromycin and colonies expressing the transgenes (4–7 colonies) were identified by immunoblotting and pooled. A similar approach was used to generate the MIA PaCa-2-Dox-NF1 cell line. To generate the MIA PaCa-2-Dox-HA-p53-PML^{KO} cell line, MIA PaCa-2-Dox-HA-p53 cells were co-transfected with LentiCRISPRv2-PML-gRNA and empty LentiCRISPRv2-blasticidin, selected with blasticidin and then seeded as single cells in 96-well to establish individual clones deleted of PML, as assessed by immunoblotting. Then, 13 Individual clones were pooled and expanded as one cell population. To generate the MIA PaCa-2-Dox-HA-p53-PML^{R} cell line, MIA PaCa-2-Dox-HA-p53-PML^{KO} cells were transduced with the bicistronic pLVX-Hyg-PML^{R} lentivirus, selected with hygromycin and all colonies were pooled and expanded as one cell population. To the generate HPDE-HA-Kras^{G12D} cell line, cells were transduced with pBABE-HA-Kras^{G12D} retroviruses, selected with puromycin and 7 clones expressing Kras^{G12D} identified by immunoblotting were pooled and expanded as one cell population. To generate the HPDE-NF1^{KO} cell line (*NF1*^{KO}), cells were transduced with LentiCRISPRv2-NF1-gRNA lentiviruses, selected with puromycin and 3 individual clones harboring *NF1* deletion identified by immunoblotting were pooled and expanded as one cell population. A similar CRISPR/CAS9 strategy was used to generate HPDE-NF1^{KO}-p53^{KO} cells with simultaneous deletion of *NF1* and *p53* (*NF1*^{KO};*p53*^{KO}) or HPDE-NF1^{KO}-PML^{KO} cells with simultaneous deletion of *NF1* and *PML* (*NF1*^{KO};*PML*^{KO}). To generate HPDE-HA-Kras^{G12D}-NF1^{KO} cells

(*KNF1*^{KO}), HPDE-HA-Kras^{G12D} cells were cotransfected with pLVX-Hyg and LentiCISPRv2-NF1-gRNA, selected with hygromycin, and then seeded as single cells in 96-well to establish individual clones deleted of *NF1*, as assessed by immunoblotting. Then, 5 individual clones were pooled and expanded as one cell population. HPDE-HA-Kras^{G12D}-NF1^{KO}-NF1^{R} (*KNF1*^{KO};*NF1*^{R}), HPDE-NF1^{KO}-p53^{KO}-NF1^{R} (*NF1*^{KO};*p53*^{KO};*NF1*^{R}) or HPDE-NF1^{KO}-p53^{KO}-p53^{R} (*NF1*^{KO};*p53*^{KO};*p53*^{R}) cell lines were established through lentiviral infection by the bicistronic pLVX-IRES-Neo-NF1^{R} or pLVX-IRES-Neo-p53^{R} expression vector as appropriate followed by selection with G418 and confirmation by immunoblotting. All colonies were then pooled and expanded as a single cell population.

METHOD DETAILS

Plasmid constructs

To generate pLVX-Tre3G-HA-p53, pLVX-Tre3G-HA-p53.R248Q, pLVX-Tre3G-HA-p53.R273H expression plasmids, cDNAs were amplified using pQCXIP-p53, pQCXIP-p53.R248Q or pQCXIP-p53.R273H as templates and cloned into pLVX-Tre3G. To generate the pLVX-Tre3G-NF1 expression plasmid, cDNAs were amplified through two successive rounds of overlapping PCR using a lambda-ZAP11 human placental cDNA library (Clontech) and cloned into pLVX-Tre3G. To generate pLVX-IRES-Neo-NF1^{R} and pLVX-IRES-Neo-p53^{R}, cDNAs were amplified using pLVX-Tre3G-NF1 and pQCXIP-p53, respectively and cloned into pLVX-IRES-Neo. To generate pCMV5-HA-PML, PMLIV was amplified by PCR using the Flag-PML IV/pRK5 plasmid as a template and cloned into pCMV5B-2xHA. To generate the pLVX-Hyg-PML^{R} construct, PMLIV cDNA was amplified by PCR using the pCMV5-HA-PML-IV plasmid as template and cloned into the pLVX-Hyg plasmid (Takara). To generate pGL3-NF1^{Luc} full-length reporter construct, a human genomic fragment corresponding to the *NF1* promoter (1,080 bp, based on NCBI NG_056197.1 and Eukaryotic Promoter Database, epd.epfl.ch, see URL1 below) was amplified by the Platinum SuperFi II DNA Polymerase-High-Fidelity using human genomic DNA obtained from HPDE cells and cloned into the pGL3-Basic plasmid. pGL3-NF1^{Luc} full-length reporter construct was used as a template to generate overlapping fragments and the resulting PCR products were cloned into the pGL3-basic plasmid. Introduction of mutations in all plasmids was conducted by site-directed mutagenesis using the QuickChange Site-Directed Mutagenesis kit according to the manufacturer's instructions (Agilent). All cloning procedures were performed using the In-Fusion® HD Cloning Plus according to the manufacturer's instructions (Takara). All cloned DNA fragments and their corresponding mutants were checked by sequencing.

URL1: https://swissregulon.unibas.ch/jbrowse/JBrowse/?data=hg19_f5&tracks=DNA%2Cgenes%2Cpromoters%2Ctfbs&loc=chr17%3A29420019..29423988&highlight=)

Mice treatment and analysis

Mice were divided into treatment groups randomly while satisfying the criteria that the average body weight in each group would be about the same. Caerulein was dissolved in 0.9% saline and injected intraperitoneally at a dose of 50 μg/kg of body weight. Blood glucose levels were measured after 6 h of fasting with blood collected from the tail vein using the *ReliON Prime* blood glucose strips. *In vivo* imaging of mice was conducted following anesthesia by isoflurane inhalation and injection of D-luciferin at 75mg/kg. Bioluminescence images were captured using a Xenogen IVIS Spectrum (Caliper Life Sciences, Hopkinton, MA). PDAC formation was confirmed by analysis of formalin-fixed paraffin-embedded (FFPE) pancreatic sections by hematoxylin and eosin (H&E) and immunohistochemistry (IHC) using anti-CK19 antibody.

Cell lines and culture

HEK293T, MIA PaCa-2 and Panc-1 cell lines (wild-type or stable) were cultured in Dulbecco's modified Eagle's medium (DMEM) supplemented with 10% fetal bovine serum (FBS) (Atlanta biologicals) and antibiotic antimycotic (Gibco). HPDE cells were cultured in Keratinocyte SFM media (Gibco), containing bovine pituitary extract, antibiotic antimycotic and epidermal growth factor (EGF). For stable cell lines, cells were cultured in their respective complete media containing G418, hygromycin, blasticidin or puromycin as appropriate. EGF was maintained in the culture media for all HPDE isogenic cell lines as they maintained dependency on EGF for cell proliferation irrespective of their genotype.

Lentiviruses were produced by transfecting HEK293T cells with the lentiviral backbone constructs and Lenti-X Packaging Single Shot system as described by the manufacturer (Takara). Lentiviral particles were harvested from the supernatant medium after a period of 48–72 h. The conditioned media were cleaned of cell debris by centrifugation at 5000xg for 15 min, filtered through a 0.45μm filter and aliquots were frozen at −80°C until use. Retroviruses were produced by transfecting HEK293T cells with retroviral backbone constructs and the packaging plasmids pCMV-VSV-G and pUMVC using X-tremeGENE9 (Roche). The conditioned media were processed as described earlier for lentiviruses except that they were used immediately after collection. Transduction of pancreatic cell lines by lentiviruses or retroviruses was conducted in the presence of 3 μg/mL or 8 μg/mL of polybrene, respectively.

To assess cell proliferation, cells were seeded in 6-well plates and cell numbers were determined using an automatic cell counter (Invitrogen). Alternatively, cells were seeded in 96-well plates and subjected to MTT assays according to manufacturer's instructions (Abcam).

Soft agar colony formation assay

Base layers consisting of growth medium (with phenol red) containing 0.6% agar were poured onto p60 dishes and allowed to solidify. A total of 5,000 cells were plated in top layers consisting of growth medium containing 0.3% agar and colonies were visualized after 2–3 weeks.

Ras-GTP pulldown assay

Tissue or cell lysates were prepared in lysis buffer (25 mM Tris-HCl, pH 7.2, 150 mM NaCl, 5 mM MgCl2, 5% glycerol and 1% NP40) supplemented with phosphatase inhibitors (Sigma) and EDTA-free protease inhibitors (Roche). According to manufacturer's instructions, tissue or cells were lysed with 1mL of lysis buffer containing GST-tagged RAF-RBD for 10 min on ice. Then, 90% of the pre-cleared lysates were added to pre-washed glutathione agarose beads for 1 h at 4°C under constant rocking. The beads were subsequently pelleted and washed 3 times with lysis buffer and eluted for immunoblotting using 1X SDS-PAGE sample buffer. The other remaining 10% of lysates were used to determine total Ras levels by immunoblotting.

Immunoblotting

Cell extracts were prepared in lysis buffer containing 50mM Tris HCl (pH = 8.0), 120mM NaCl, 5mM EDTA, 1% Igepal, protease inhibitors (Roche Diagnostics) and phosphatase inhibitors (Calbiochem). Protein concentrations were determined using the Bradford reagent (Sigma-Aldrich) and samples were denatured using SDS sample buffer (Invitrogen). Samples were loaded into a NuPAGE Bis-Tris Gel (Invitrogen) and separated by electrophoreses at 200 V. The gels were then transferred onto a nitrocellulose membrane (BioRad) by a wet transfer system (BioRad) and blocked by incubation with 5% dry milk in TBST (TBS with 0.2% Tween20). Membranes were probed with the primary antibody for 2 h at room temperature in the blocking buffer, washed with TBST and incubated with the appropriate peroxidase-conjugated secondary antibody. Enhanced chemiluminescence (ECL) western blotting substrates (Pierce) were used for visualization of the bands. For blot imaging and densitometric analysis, the chemiluminescent blots were imaged with the ChemiDoc MP imager (Bio-Rad). The band analysis tools of ImageLab software version 4.1 (Bio-Rad) were used to select and determine the background-subtracted density of the bands in all blots, including the loading controls. For background subtraction, a value of 1 was used while imaging the blots for the total protein measurements from the lanes. Quantification of specific proteins was determined based on the normalization with the corresponding loading control.

Immunofluorescence and immunohistochemistry

Tissue samples were fixed in 10% formalin and embedded in paraffin. Three to six sections were generated from each block and a representative section from at least 6 mice was selected in a random/blinded manner in order to achieve unbiased analysis of data. Tissue sections were then deparaffinized with xylene and rehydrated in a graded series of ethanol. Antigen-retrieval was performed for 10 min at high temperature in citrate buffer. For IHC, endogenous peroxidase inhibition was carried in 10% H_2O_2 in water. Then, slides were blocked and incubated overnight with the appropriate primary antibody or IgG-matched isotype control antibody (negative control) at 4°C. For immunofluorescence, slides were incubated with the secondary antibodies conjugated to Alexa-Fluor®568 or Alex-Fluor®448, co-stained with DAPI and viewed with a Nikon Ti-E fluorescence microscope. IHC was done with the VECTASTAIN Elite ABC HRP kit as per manufacturer's instructions (Vector Laboratories) and color development was done with the DAB Peroxidase Substrate kit with or without nickel added enhancement as appropriate.

For tissue histology, paraffin sections were stained with H&E using standard techniques and cross-sectional areas were examined in at least six animals for each determination.

For human sample analysis, we utilized three independent TMAs (n = 3) comprising 179 samples confirmed either as normal (65) or PDAC (114) with both PanINs and full PDAC lesions (as gauged by H&E staining). NF1 or p53 expression was probed using highly specific anti-NF1 and anti-p53 antibodies. Then, the relative expression levels of NF1 or p53 in the three TMAs were scored in a blinded manner by two independent investigators as low or high (including all samples in a given TMA). Then, the percentages of samples with NF1-high, NF1-low, p53-high or p53-low in each TMA were determined independently. The results corresponding to the three TMA (n = 3) were either presented as mean ± SEM of percentages of samples with NF1-high or NF1-low expression or as mean ± SEM of the percentages of overlapping samples relative to the levels of expression of NF1 and p53 (e.g., NF1-high/p53-high, NF1-low/p53-low, NF1-high/p53-low, NF1-low/p53-high). The numbers of samples analyzed are presented in tables within the appropriate figures.

Real-time PCR (RT-PCR)

Total RNA was extracted from tissues or cultured cells using TRIzol (ThermoFisher), purified with RNeasy minicolumns (QIAGEN) and reverse transcribed using a High-Capacity cDNA Reverse Transcription kit (Applied Biosystems). The resulting cDNA was analyzed by RT-PCR. Briefly, 25 ng of cDNA and 150 nmol of each primer were mixed with SYBR GreenER qPCR SuperMix (Invitrogen). Reactions were performed in the 96-well format using an ABI PRISM 7900HT instrument (Applied Biosystems). Relative mRNA levels were calculated using the comparative Ct method and normalized to *GAPDH* mRNA.

Primers used for human samples:
KRAS-For: 5'-CAGTAGACACAAAACAGGCTCAG-3'
KRAS-Rev: 5'-TGTCGGATCTCCCTCACCAATG-3'
NF1-For: 5'-GCCTTGAGGAAAACCAGCGGAA-3'
NF1-Rev: 5'-TCCTACTGCACCGATGCTGTTC-3'
GAPDH-For: 5'-CCATGGGGAAGGTGAAGGTC-3'
GAPDH-Rev: 5'-AGTGATGGCATGGACTGTGG-3'
Primers used for mouse samples:
NF1-For: 5'-TCAAGCATGGACTTGGCACT-3'
NF1-Rev: 5'-CATTCGTATTGCTGGGTGCG-3'
p53-For: 5'-GGGACAGCCAACTCTGTTATGTGC-3'
p53-Rev: 5'-CTGTCTTCCAGATACTCGGGATAC-3'
Gapdh-For: 5'-CACCATCTTCCAGGAGCGAG-3'
Gapdh-Rev: 5'-CACCATCTTCCAGGAGCGAG-3'

Chromatin immunoprecipitation assay (ChIP)

ChIP assays were performed using a chromatin immunoprecipitation assay kit following the manufacturer's instructions (Millipore). Briefly, chromatin was extracted from tissue or cells, sonicated and immunoprecipitated with antibodies against PML, p53 or isotype-matched control IgG. PCR was run on the chromatin and the products were analyzed on a 2% agarose gel. Relative DNA binding was determined by classical qPCR.[47,48] The following primers were used:

Primers for human ChIP
NF1-For: 5'- TAACTTCCAACTCCGGGAGCA-3'
NF1-Rev: 5'- GAGGTGACGTCATCTAACTCCT-3'
GAPDH-For: 5'CGGGATTGTCTGCCCTAATTAT-3'
GAPDH-Rev: 5'GCACGGAAGGTCACGATGT-3'
Primers for mouse ChIP
NF1-For: 5′-AGCCTCAGGACACCCTAACTTCTA -3'
NF1-Rev: 5′-GCGGGTCTCCCCACCTAAACT -3'
Gapdh-For: 5′-ATCCACGACGGACACATTGG-3′
Gapdh-Rev: 5′-TGGTGCTGCCAAGGCTGTGG-3′

Luciferase reporter assay

MIA PaCa-2 or MEF cells were plated in 6-well plates and transfected with the NF1 luciferase reporter constructs in the absence or presence of pQCXIP-p53 mutants using X-tremeGENE9. The pRL-SV40 plasmid (Promega) was cotransfected as a normalization control. Cells were incubated for 24 h with the transfection mixtures and allowed to recover for another 24 h before measuring luciferase activity using the Dual-Luciferase Reporter Assay kit (Promega). Firefly Luciferase activity was normalized on the basis of Renilla luciferase expressed from the pRL-SV40 plasmid.

Analysis of public datasets

NF1, *KRAS*, *TP53*, *p16INK4A* and *SMAD4* mutational status data were downloaded from public datasets, including The Cancer Genome Atlas (TCGA, also known PAAD-US), Pancreatic Cancer Australian (PACA-AU), Pancreatic Cancer Canada (PACA-CA) and other genomic published studies (GPS). Analysis of TCGA dataset was achieved through accessing TCGA Data Portal (URL2 provided below). Analysis of the PACA-CA and PACA-AU datasets was achieved through accessing the International Cancer Genome Consortium (ICGC) Data Portal (URL3 provided below). Table S1 provides the PMID of all genomic published studies used in this study. All data were downloaded after searching for *NF1* and pancreatic ductal adenocarcinoma, which yielded data for 1,471 PDAC samples. Each patient sample was then assessed whether its harbors mutations in *NF1*, *KRAS*, *TP53*, *p16INK4A* or *SMAD4*, and different colors were used to highlight the different mutations in Table S1. The impacts of missense mutations on NF1 protein activity were predicted using the PolyPhen-2 prediction tool (URL4 provided below). The predicted impacts and their corresponding scores as well as nonsense and missense mutations are highlighted in yellow in Table S1. The two isoforms of NF1 used in the analysis are AAV50004.1 and AAA59925.1.

URL2: https://portal.gdc.cancer.gov/genes/ENSG00000196712?canDistTable_size=100
URL3: https://dcc.icgc.org/genes/ENSG00000196712/mutations
URL4: http://genetics.bwh.harvard.edu/pph2/

QUANTIFICATION AND STATISTICAL ANALYSIS

For all experiments, the sample size was determined empirically (preliminary experiments were performed) to ensure that the desired statistical power could be achieved. All values are expressed as mean ± SEM. The error bars (SEM) shown for all results were derived from biological replicates, not the same sample replicates. Significant differences between two groups were evaluated using a two-tailed, unpaired t-test, which was appropriate for the statistics, as the sample groups displayed a normal distribution and comparable variance. The chi-square test was used to test the independence of the samples in the three independent human PDAC TMAs. Statistical significance values are presented as follow: ns (not significant), $p < 0.05$, $p < 0.01$ or $p < 0.001$. Statistical significance of survival differences was determined by log-rank test.